

CEBAF Program Advisory Committee Eight Cover Sheet

This proposal must be received by close of business on Thursday, April 14, 1994 at:

CEBAF

User Liaison Office, Mail Stop 12 B

12000 Jefferson Avenue

Newport News, VA 23606

Proposal Title

Polarization Measurements of Neutral Pion Photoproduction: A Test of Chiral Dynamics

Contact Person

Name: Blaine Norum

Institution: UVA

Address: Department of PHYSICS

Address: McCormick Road

City, State ZIP/Country: Charlottesville, VA 22902

Phone: (804) 924-6789

FAX: (804) 924-4576

E-Mail → Internet: Blaine@Theory.Phys.Virginia.edu

Experimental Hall: 8

Total Days Requested for Approval: 17

Minimum and Maximum Beam Energies (GeV): 2.3

Minimum and Maximum Beam Currents (μ Amps): 5

CEBAF Use Only

Receipt Date: 4/17/94 11:00 AM

By: [Signature]

HAZARD IDENTIFICATION CHECKLIST

CEBAF Experiment: _____

Date: April 13, 1994

Check all items for which there is an anticipated need—do not check items that are part of the CEBAF standard experiment (HRSE, HRSR, CLAS, HMS, SOS in standard configurations).

<p>Cryogenics</p> <p>_____ beamline magnets</p> <p>_____ analysis magnets</p> <p><input checked="" type="checkbox"/> target</p> <p>_____ drift chambers</p> <p>_____ other</p>	<p>Electrical Equipment</p> <p><input checked="" type="checkbox"/> cryo/electrical devices</p> <p>_____ capacitor banks</p> <p>_____ high voltage</p> <p>_____ exposed equipment</p>	<p>Radioactive/Hazardous Materials</p> <p>List any radioactive or hazardous/toxic materials planned for use:</p> <p>_____</p> <p>_____</p>
<p>Diagnostic Monitors</p> <p>_____ inside diameter</p> <p>_____ operating pressure</p> <p>_____ window material</p> <p>_____ window thickness</p>	<p>Flammable Gases/Liquids (incl. target)</p> <p>type: <u>Hydrogen</u></p> <p>flow rate: _____</p> <p>capacity: _____</p>	<p>Other Target Materials</p> <p>_____ Beryllium (Be)</p> <p>_____ Lithium (Li)</p> <p>_____ Mercury (Hg)</p> <p>_____ Lead (Pb)</p> <p>_____ Tungsten (W)</p> <p>_____ Uranium (U)</p> <p>_____ Other (list below)</p> <p>_____</p> <p>_____</p>
<p>Vacuum Vessels</p> <p>_____ inside diameter</p> <p>_____ operating pressure</p> <p>_____ window material</p> <p>_____ window thickness</p>	<p>Radioactive Sources</p> <p>_____ permanent installation</p> <p>_____ temporary use</p> <p>type: _____</p> <p>strength: _____</p>	<p>Large Mech. Structure/System</p> <p>_____ lifting devices</p> <p>_____ motion controllers</p> <p>_____ scaffolding or elevated platforms</p> <p>_____ other</p>
<p>Lasers</p> <p>type: <u>Ar-ion</u></p> <p>wattage: <u>25</u></p> <p>class: <u>IV</u></p> <p>Installation</p> <p><input checked="" type="checkbox"/> permanent</p> <p>_____ temporary</p> <p>Use</p> <p>_____ calibration</p> <p>_____ alignment</p> <p><input checked="" type="checkbox"/> photon source</p>	<p>Hazardous Materials</p> <p>_____ cyanide plating materials</p> <p>_____ scintillation oil (from)</p> <p>_____ PCBs</p> <p>_____ methane</p> <p>_____ TMAE</p> <p>_____ TEA</p> <p>_____ photographic developers</p> <p>_____ other (list below)</p> <p>_____</p> <p>_____</p> <p>_____</p>	<p>Notes:</p> <p><u>Requires installation of</u></p> <p><u>detector in front of CLAS.</u></p> <p>_____</p> <p>_____</p> <p>_____</p> <p>_____</p> <p>_____</p>

Polarization Measurements of Neutral Pion Photoproduction: A Test of Chiral Dynamics

D. Crabb, B. E. Norum, D. Počanić
University of Virginia
Charlottesville, VA 22901

A. Bernstein, H. Merkel
M.I.T.
Cambridge, MA 02139

A. W. Stetz, T. P. Welch
Oregon State University
Corvallis, OR 97331

H. Crannell, J. O'Brien, D. Sober
Catholic University of America
Washington, DC 20064

C. Keppell
Virginia Union University
Richmond, VA 23220

R. Miskimen
University of Massachusetts
Amherst, MA 01003

R. Rossmanith
CEBAF
Newport News, VA 23606 and
University of Virginia

The Hall B Collaboration

April 25, 1994

Abstract

We are proposing to measure near-threshold π^0 photo-production using linearly polarized photons. Under the reasonable assumptions a) that close to threshold only s- and p-waves contribute and b) that the phases of the p-wave amplitudes are negligible we will be able to determine uniquely the amplitudes contributing to this fundamental process. We will also be able to determine the near-threshold energy dependence of the multipoles and the s-wave πN scattering length. In addition to providing precise data (previously unattainable) on a fundamental process, these measurements will permit a rigorous test of the predictions of Chiral dynamics. This experiment will be the first experiment to utilize a Compton polarized photon source in Hall B.

Contents

1	Introduction	3
2	Previous Measurements	6
3	Threshold Photo-production with Polarized Beams and Targets	13
4	The $H(\vec{\gamma}, \pi^0)$ Experiment	17
4.1	Compton Polarized Photon Source	19
4.2	Tagging Spectrometer	26
4.3	Target	27
4.4	Detector	28
5	Simulations	30
6	Beam Time Request	33
	References	37
	Appendices	40
A	New Tests of Chiral Dynamics	40
B	Experimental Observables	55

C	Future Measurements of the $p(\gamma, n)\pi^+$ Reaction	57
C.1	Kinematics and Detector Resolution	59
C.2	Neutron Detector	62
C.3	Calibration of the Neutron Detection Efficiency	64
C.4	Count rate estimates	64
C.5	Conclusion	67

1 Introduction

The fundamental nature of threshold pion photo- and electro-production processes has long been recognized.[1] This is due to the fact that the pion is nearly the Goldstone boson of QCD.[2] Starting with the low energy theorems of current algebra[3, 4] predictions for the s-wave amplitudes for the $N(\gamma, \pi)$ reaction were made.[1, 5] Later, an effective field theoretic technique called chiral perturbation theory (or chiral dynamics) was employed as a low energy approximation to QCD.[6, 7, 8, 9] The lowest, or tree level, approximation generally reproduces the results of current algebra.

Chiral perturbation theory has been employed to calculate the amplitudes for the threshold photo- and electro-production of charged and neutral pions.[10, 11] These calculations, like most, focus on the magnitudes of the s- and p-wave amplitudes surviving near threshold. Precise measurements of these magnitudes would provide stringent tests of these calculations. In addition, it was recently pointed out that the relative phases between the amplitudes are also of fundamental significance.[12] Due to time reversal invariance and S matrix unitarity they are uniquely sensitive to the low energy πN interaction.[12] Measurement of these phases will enable one to determine $a(\pi^{-0,+}N)$, the s-wave πN scattering lengths, for the first time. The conventional technique of measuring scattering lengths by very low energy scattering is not practical since neither charged pion beams with very low energies nor π^0 beams with any energy are possible. Such data will enable one to test the various predictions for the scattering lengths.[3, 9, 13] In addition, the data on previously inaccessible charge states (e.g., $\pi^0 p$ and $\pi^+ n$) will enable one to test the predicted breakdown of isospin symmetry[12] due to the mass differences of the up and down quarks.[9, 13, 8]

Previous measurements of the threshold $p(\gamma, \pi^0)$ reaction have been performed at Saclay[14] and at Mainz.[15] After some initial confusion it was realized that these data are in agreement[16, 17] with the predictions of the low energy theorems[5, 18, 19] for the s-wave electric dipole threshold amplitude E_{0+} . However, there are still several important uncertainties. These data do not unambiguously determine the energy dependence of the s-wave

amplitude E_{0+} nor do they determine the magnitudes of the p-wave multipoles (see Sec. 2).

Comparisons of the theoretical and experimental results for the threshold $N(\gamma, \pi)$ reactions are presented in Table 1. One notes that it is important to carry out the chiral perturbation theory to two loops. This is due to the effects of different $p(\gamma, \pi^0)$ and $p(\gamma, \pi^+)n$ thresholds which enter the chiral perturbation calculations at the two loop level. The two loop results shown in Table 1 are based on approximate calculations. A more rigorous evaluation of the two loop effects still has to be performed.

We note in Table 1 that measurements for the charged pion reactions, [20, 21, 22] are all about 20 years old. They are all characterized by modest resolution which results in large and difficult-to-estimate systematic uncertainties in the extraction of the amplitudes. Accordingly, there is pressing need for a modern, high precision measurement of these fundamental amplitudes and for a more precise measurement of the $p(\gamma, \pi^0)$ threshold amplitude (as well as its energy dependence).

Table 1: Threshold E_{0+} multipoles in units of $10^{-3}/m_\pi$

Channel	Low Energy Theorems	Chiral Perturbation Theory[10]	Experiment
$\gamma p \rightarrow \pi^0 p$	-2.28	$-1.33 \pm 0.09^{(a)}$ $-1.97^{(c)}$	$-2.0 \pm 0.2^{(b)}$
$\gamma p \rightarrow \pi^+ p$	26.3	$28.4^{(a)}$	27.9 ± 0.5 [20] 28.8 ± 0.7 [21]
$\gamma n \rightarrow \pi^0 n$	0.50	$0.62 \pm 0.09^{(a)}$	
$\gamma n \rightarrow \pi^- p$	-31.3	$-31.1^{(a)}$	-31.4 ± 1.3 [21] -32.2 ± 1.2 [22]

(a) 1 loop calculation.

(b) Refs. [16] and [23] based on the Mainz data.[15]

(c) approximate 2 loops calculation.

Previous measurements of the $p(\gamma, \pi^0)$ reaction were of the unpolarized (target and γ 's) cross section only. These data do not unambiguously determine the energy dependence of the s-wave amplitude E_{0+} or the magnitude of the p-wave multipoles (see Sec. 3). In order to determine these one needs to make polarization measurements (see Appendix B and Sec. 3). The experiment proposed here (using polarized γ 's and an unpolarized target) constitutes the first step towards filling this gap. The next step will be to perform an experiment using polarized γ 's with a polarized proton target. With the reasonable assumptions a) that only s- and p-wave pions contribute close to the threshold and b) that the relative phases of the p-wave amplitudes are negligible, this will constitute a complete measurement of the multipoles. With these data we will test the predictions of chiral perturbation theory (low energy QCD) for the threshold π photoproduction multipoles as has been previously discussed. In addition, we will determine the slopes of the threshold multipoles and the s-wave $\pi^0 N$ scattering length (see ref. [12] and Appendix A).

The experiments discussed here require the construction of the Compton backscattering facility. It was therefore considered prudent to proceed one step at a time. We request here the beam time to inaugurate the program and the facility with a measurement of the threshold $p(\vec{\gamma}, \pi^0)$ reaction using linearly polarized γ 's and an unpolarized target. These measurements will provide important new data on the near-threshold s- and p-wave amplitudes while being a relatively straightforward commissioning experiment. Following this we will propose measurements of the threshold $p(\gamma, \pi^0)$ reaction using polarized γ 's and polarized targets. These measurements will determine the pattern of isospin breaking in the $N(\gamma, \pi)$ reaction as well as the scattering length for the $n\pi^+ \rightarrow p\pi^0$ charge exchange reaction (see ref. [12] and Appendix A). We will also propose measurements of the $p(\gamma, \pi^+)n$ reaction with polarized photons and unpolarized targets. These measurements will determine the threshold s- and p-wave amplitudes to test the predictions of chiral perturbation theory[10] and will be important to the interpretation of the phase measurement in the $p(\gamma, \pi^0)$ reaction.

The proposal presented here makes unique use of the CEBAF beam. To make this proposal feasible we require a 2.3 GeV, CW beam. The Compton $\vec{\gamma}$ source will have the required brightness to perform a precision experiment

along with the added advantages of large and controlled γ polarization. In addition, there will be fewer incident photons below pion threshold. This will enable us to run at high rates with less competing electromagnetic backgrounds.

2 Previous Measurements

Previous measurements of the unpolarized cross sections for the $p(\gamma, \pi^0)$ reaction were performed at Saclay[14] with a 1% duty cycle accelerator and at Mainz [15] with a CW accelerator. The results from the two laboratories are in agreement within the experimental errors. Since the results from Mainz are much more accurate they will be the only ones referred to here.

To compare theory and experiment one needs to define[1] the multipole amplitudes. At threshold only the electric dipole amplitude E_{0+} is not zero since this leads to the emission of s-wave pions. There are three multipoles (M_{1+} , M_{1-} , and E_{1+}) for which the pions are emitted in p-waves. The notation is the E(M) signifies electric (magnetic) character for the photon, the integer refers to the pion's angular momentum and \pm refers to the total angular momentum $j = \ell \pm 1/2$.

With the safe assumption that the pions are emitted in s- or p-waves close to threshold one can write the expression for the unpolarized cross section as:

$$\begin{aligned}
 \sigma(\theta_\pi^*) &= (p_\pi^*/k^*) (A + B \cos \theta_\pi^* + C \cos^2 \theta_\pi^*) \\
 \sigma_{tot} &= 4\pi(p_\pi^*/k^*) [A + C/3] \\
 A &= |E_{0+}|^2 + |r|^2 \\
 B &= 2\Re(E_{0+}^* z) \\
 C &= |z|^2 - |r|^2
 \end{aligned} \tag{1}$$

where p_π^* and k^* represent the pion and photon CM momentum, r and z are linear combinations of the p-wave multipoles:

$$\begin{aligned}
 z &= 3E_{1+} + M_{1+} - M_{1-} \\
 2|r|^2 &= |2M_{1+} + M_{1-}|^2 + |3E_{1+} - M_{1+} + M_{1-}|^2
 \end{aligned} \tag{2}$$

Near threshold, due to the angular momentum barrier, the momentum dependence of the p-wave multipoles can be characterized as:

$$M_{1+}, M_{1-}, E_{1+} \sim p^* = p_\pi^* k^* / m_\pi^2 \quad (3)$$

where the factor of m_π^2 has been included for convenience. It can be seen that at threshold the contribution of the p-wave multipoles vanishes and sufficiently close to threshold the s-wave multipole E_{0+} dominates.

There has been some confusion about the interpretation of the original[14] Saclay and Mainz[15] experiments. In the original papers a substantial disagreement with the predictions of the low energy theorems was claimed.[14, 15] This was due in part to a theoretical ambiguity because the low energy theorems assumed isospin conservation and therefore a common threshold for the $p(\gamma, \pi^0)$ and $p(\gamma, \pi^+)n$ reactions, in contrast with the experimental difference of 6.8 MeV. Therefore it was not clear at which threshold to apply the low energy theorem. This was subsequently cleared up by Naus who showed that the low energy theorems should be applied at the primary $p(\gamma, \pi^0)$ threshold of 144.7 MeV.[18, 19]

Another difficulty in the analysis of the experiments was the ambiguity in the extraction of the s- and p-wave multipoles. As a consequence of eq. 3 it was pointed out that the measured total cross sections depend primarily on the s-wave multipole E_{0+} close to threshold; the values extracted in this way[16, 17] agree with the predictions of the low energy theorems. Further from threshold an ambiguity exists which will be discussed below.

There are currently two analyses of the Mainz data.[24, 23] Both analyses assumed eq. 3 for the energy dependence of the p-wave multipoles. This is a significant improvement over the original Mainz analysis[15] which did not assume this constraint. The extracted values for the p-wave multipoles were not in agreement with eq. 1 which is indicative of the fact that the data are not sufficiently accurate (or extensive) to determine the p-wave multipoles. The results of the two analyses differ because there are two minima in the χ^2 surface. The analysis of Drechsel and Tiator[24] found the minimum in which the magnitude of the p-wave multipoles are close to those assumed by the original Mainz analysis[15] and to the theoretical p-wave multipoles.[24, 25] There is actually a slightly deeper minimum for which the p-wave multipoles

are smaller.[23] The results are presented in figs. 1, 2, and 3 and compared to the Mainz data.

The differential cross sections are presented in fig. 1 with the fits discussed above. The original Mainz analysis[15] fit to the general form of the eq. 1 and extracted the A, B, and C coefficients. The fits obtained by the other analyses are also shown. Except for the lowest energy where the χ^2 value of Drechsel and Tiator[24] is larger the fits are all of the same quality.

The total cross section is shown in fig. 2 with the p-wave contribution of each solution. Since the total cross section is the sum of the s- and p-wave components this means there is a significant difference for the s-wave component in the two solutions. This is shown in fig. 3 where the values for E_{0+} are shown. The two analyses extrapolate to the same value at threshold but have a significantly different energy dependence. The comparison to the predictions of chiral perturbation theory with approximate two loop contributions[6, 7, 8, 9] is shown. It is clearly of great interest to clarify the experimental energy dependence in order to compare with theory. It is also very interesting to obtain small errors to see if the predicted unitary cusp at the $p(\gamma, \pi^+)n$ threshold[25] can be observed.

The measured differential cross section for the $p(\gamma, \pi^0)$ reaction for a photon energy of 151 MeV are shown in fig. 4. It can be seen that the theoretical predictions[10, 25] have too large a forward-backward asymmetry indicating a p-wave contribution which is too large.

An improved version of the Mainz experiment was carried out in the TAPS photon detector in the spring of 1992.[26] We anticipate that the analysis will be completed this summer and may help to resolve some of the ambiguities presented above. However we note that an experiment with linearly polarized photons and an unpolarized target is required to sort out all of the p-wave multipoles. This is the subject of the present proposal.

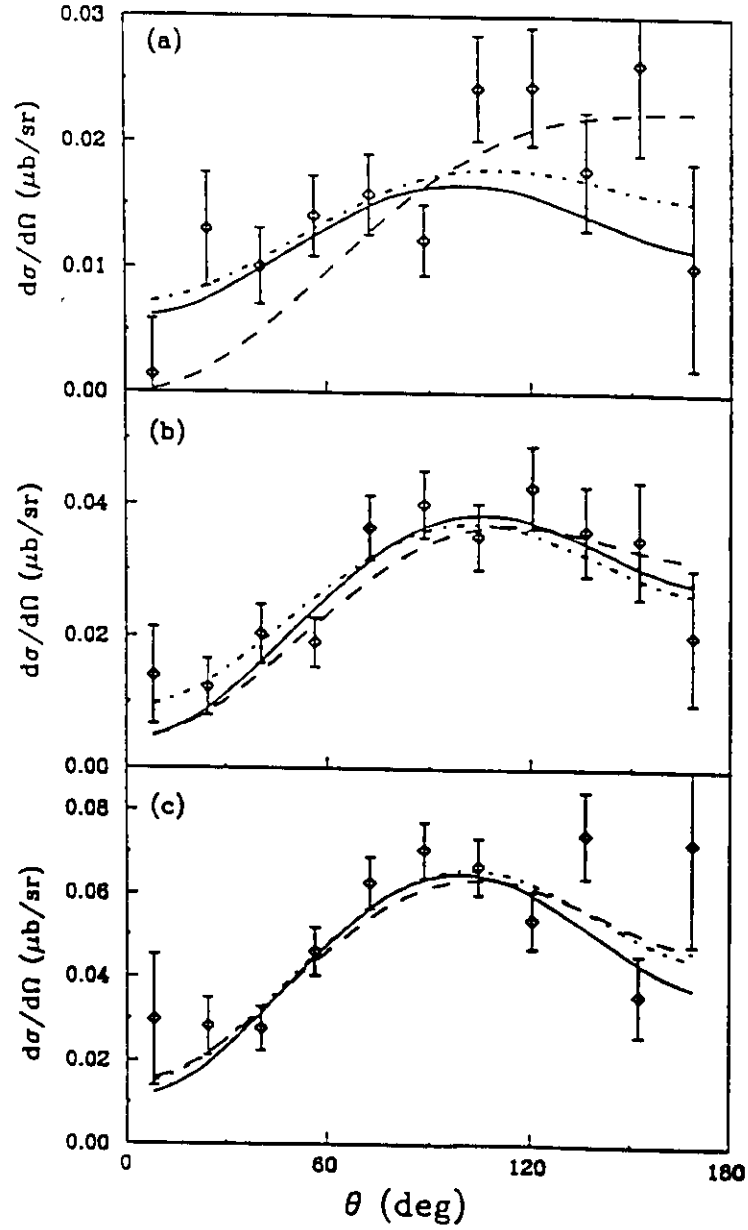


Figure 1: Differential cross sections for the $p(\gamma, \pi^0)$ reaction[15] at (a) 146.8 MeV; (b) 149.1 MeV; and (c) 151.4 MeV. The solid lines are the fits of the Mainz group[15] for the A, B, and C coefficients of eq. 2. The dashed[24] and dotted curves[23] are empirical multipole fits.

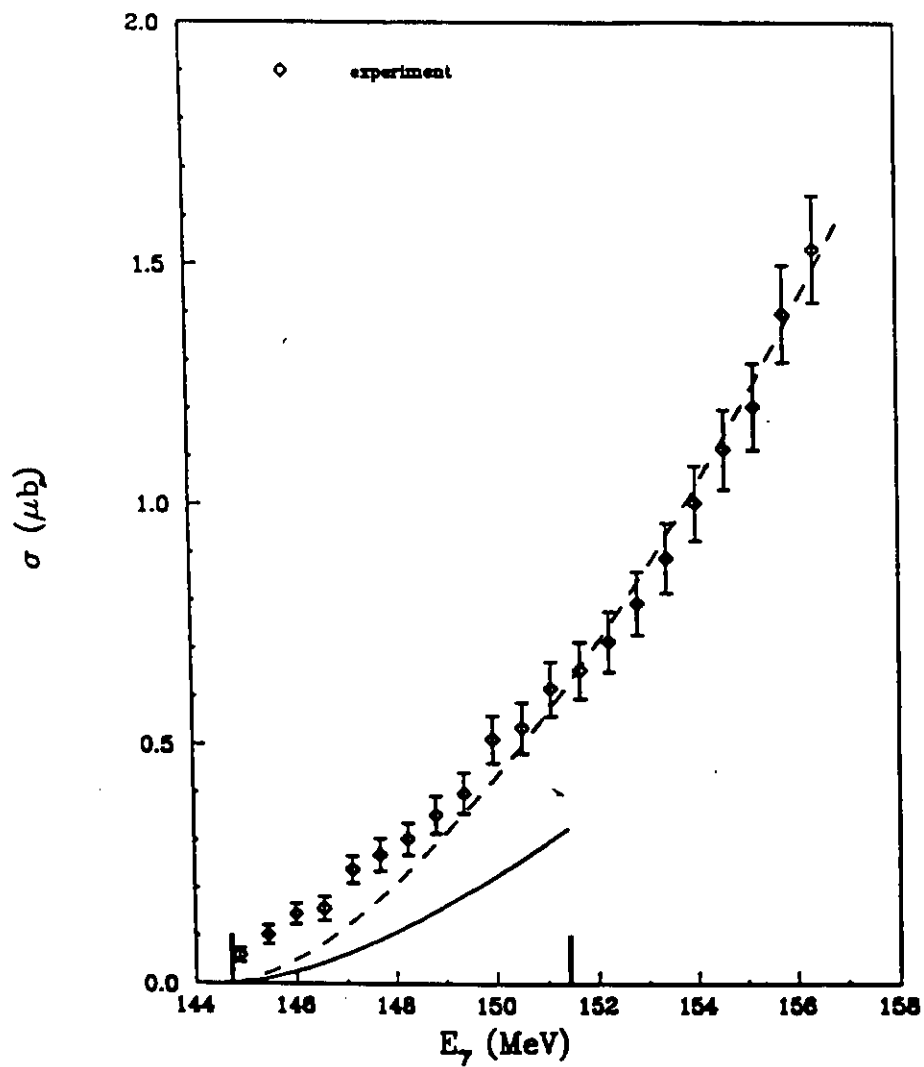


Figure 2: Total cross sections for the $p(\gamma, \pi^0)$ reaction.[15] The dashed[24] and solid[23] curves are the p-wave contribution from the two empirical multipole solutions. The difference between the total cross section and the p-wave contribution is due to the s-wave contribution.

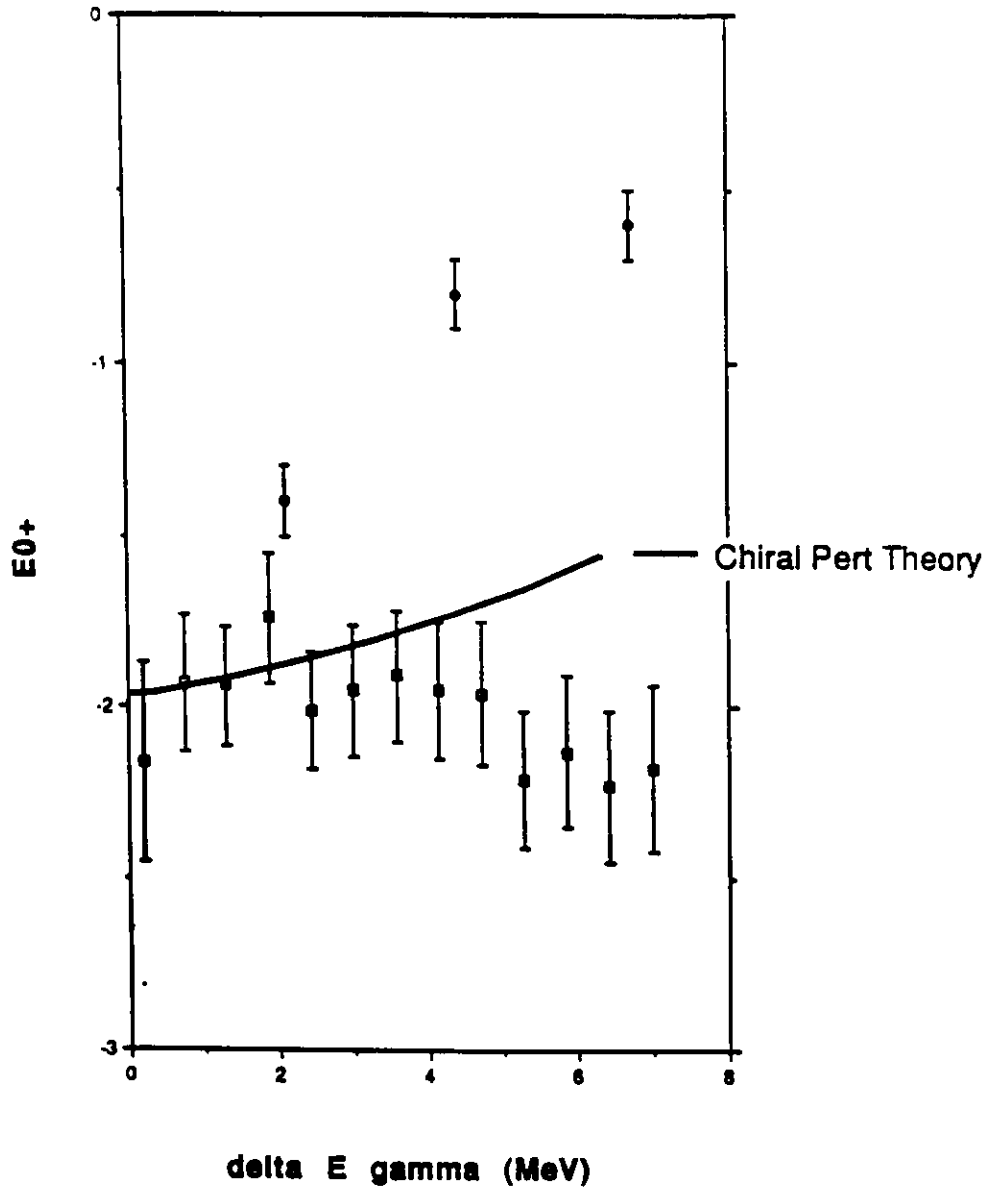


Figure 3: E_{0+} (in units of $10^{-3}/m_\pi$) for the $p(\gamma, \pi^0)$ reaction. The solid[23] and circular[24] points with the errors are from the empirical multipole analyses. The solid curve is the prediction of chiral perturbation theory with an approximation to the two loop, isospin breaking, effects.[10]

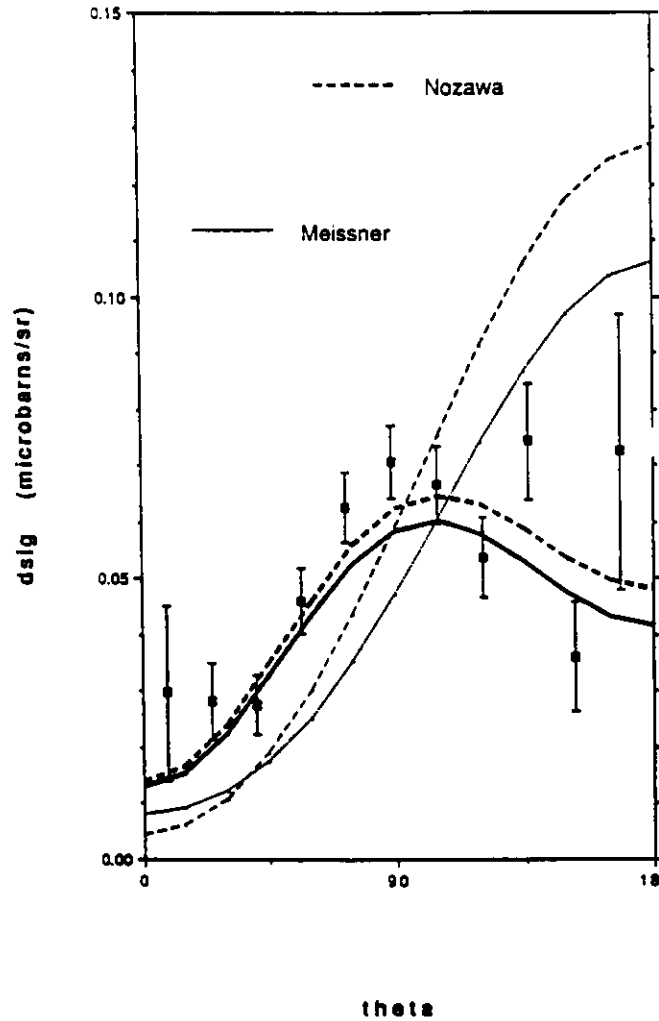


Figure 4: Differential cross section for the $p(\gamma, \pi^0)$ reaction at 151 MeV. The Mainz data[15] are shown with the predictions of chiral perturbation theory (dotted line),[10] a πN interaction model (light dashed line),[25] and the empirical fits. The heavy dashed[24] and solid[23] curves are the empirical multipole fits.

3 Threshold Photo-production with Polarized Beams and Targets

In Sections 1 and 2 we have presented the physics motivation for the proposed measurements and a summary of the experimental status of the unpolarized threshold photoproduction experiment. At this time there are no experiments with either polarized beams or targets. The formalism for the observables with polarization[24, 27, 28] in terms of the multipoles is presented in App. B. In this section the results will be given in summarized form to make the physics more transparent.

The cross section for the differential cross section for linearly polarized photons with a polarized proton target is:

$$\begin{aligned} \sigma(\theta_\pi^*, \phi_\pi^*) &= \sigma_0(\theta_\pi^*) \{1 + \Pi_\gamma \Sigma(\theta_\pi^*) \sin 2\phi_\pi^* \\ &+ P_T T(\theta_\pi^*) \cos \phi_\pi^* + P_T \Pi_\gamma (H(\theta_\pi^*) \sin \phi_\pi^* \cos 2\phi_\pi^* \\ &+ P(\theta_\pi^*) \cos \phi_\pi^* \sin 2\phi_\pi^*)\} \end{aligned} \quad (4)$$

where θ_π^*, ϕ_π^* are the pion CM angles and:

1. $\sigma_0(\theta_\pi^*)$ is the unpolarized cross section (eqs. 2 and 3);
2. $\Sigma(\theta_\pi^*)$ is the asymmetry for polarized photons with magnitude Π_γ (independent of the target polarization);
3. $T(\theta_\pi^*)$ is the asymmetry for a target polarized normal to the reaction plane with magnitude p_T (independent of the photon polarization); and
4. $H(\theta_\pi^*)$ and $P(\theta_\pi^*)$ are the asymmetries when both target and photon are polarized (double polarization).

In the proposed experiment we will employ polarized photons with an unpolarized liquid hydrogen target and measure $\sigma_0(\theta_\pi^*)$ and $\Sigma(\theta_\pi^*)$. From eqs. 1 and 2 we note that there are three different linear combinations of the four s- and p-wave multipoles (E_{0+} , M_{1+} , M_{1-} , and E_{1+}). From the unpolarized cross section alone these cannot be unambiguously determined. The measurement

of $\Sigma(\theta_\pi^*)$ will completely determine the amplitude of the four multipoles. The sensitivity of this observable to the different multipole sets[10, 24, 23, 25] is presented in fig. 3 for a photon energy of 151 MeV. We note that there are differences of sign between the predictions of the theoretical models[10, 25] and the empirical multipole sets,[24, 23] as well as large differences in magnitude. Differentiating between these sets will be straightforward.

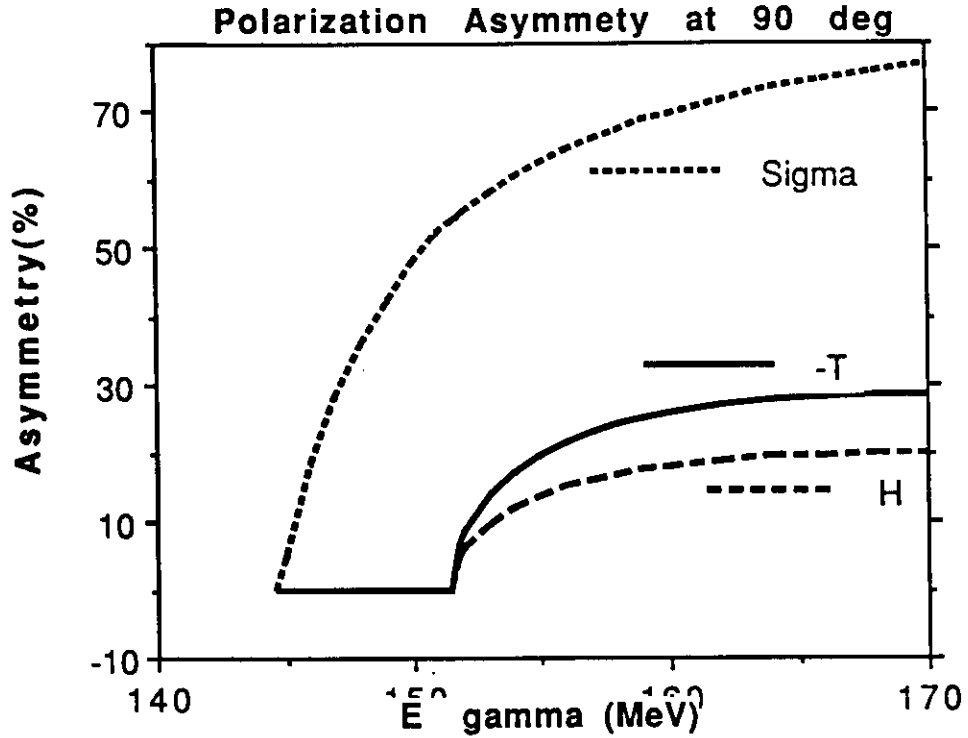


Figure 5: The polarized photon asymmetry for the $p(\gamma, \pi^0)$ reaction at 151 MeV. The heavy solid[23] and heavy dashed[24] upper curves are from empirical multipole fits to the unpolarized cross section. The light solid and light dotted curves are the predictions of chiral perturbation theory[10] and a πN interaction model of Nozawa *et al.*

Once the magnitudes of the multipoles are measured we will be able to turn our attention to the phase measurement which will be the subject of a future proposal. In this case we will employ the polarized photon source with a

polarized target. The two target-polarization observables can be expressed as(Appendix B):

$$\begin{aligned} T(\theta_\pi^*)\sigma_0(\theta_\pi^*) &\cong 3(p_\pi^*/k^*) \sin \theta_\pi^* \Im s(1, -1, 0) \\ H(\theta_\pi^*)\sigma_0(\theta_\pi^*) &\cong \cos(\theta_\pi^*)P(\theta_\pi^*) \cong -(p_\pi^*/k^*) \sin \theta_\pi^* \cos \theta_\pi^* \Im s(3, 1, 2) \end{aligned} \quad (5)$$

where we have made the mild approximation that the p-wave phases are negligible[29] and have introduced the notation $s(\alpha, \beta, \gamma)$ for the s-p interference amplitudes:

$$s(\alpha, \beta, \gamma) = E_{0+}^*(\alpha E_{1+} + \beta M_{1+} + \gamma M_{1-}) \quad (6)$$

The fact that it is the imaginary part of $s(\alpha, \beta, \gamma)$ that enters these target polarization observables is the crucial point since:

$$\Im s(\alpha, \beta, \gamma) = |E_{0+}| |\alpha E_{1+} + \beta M_{1+} + \gamma M_{1-}| \sin(\delta_s - \delta_p) \quad (7)$$

where $\delta_s(\delta_p)$ is the s-wave (p-wave) πN phase shift. Since $\delta_p \ll \delta_s$ [see e.g., ref. [29]] a measurement of either $T(\theta_\pi^*)$ or $H(\theta_\pi^*)$ would constitute a measurement of the s wave πN phase shift. Measuring both of them will add a strong check of our systematic error. This depends on a measurement of the magnitudes of the multipoles in phase 1 of the experiment. The magnitudes of the cross sections for polarized photons incident on polarized targets are presented in fig. 3 for $\theta_\pi^* = 90^\circ$ as a function of photon energy. One notes that they all rise rapidly with energy and that the polarization cross sections are significant in magnitude compared to the unpolarized cross section. Note that the target polarization cross sections are negligible below the $p(\gamma, \pi^+)n$ threshold at 151.4 MeV. For simplicity these calculations are presented for one of the empirical multipole sets.[23] The results of the different multipoles would differ as shown in figs. 4 and 3. The polarization asymmetries are presented in fig. 3 for $\theta_\pi^* = 90^\circ$ as a function of photon energy. Note that the polarized target asymmetries and cross sections are very small below the $p(\gamma, \pi^+)n$ threshold at 151.4 MeV. The reason for this is that the phase of the s wave amplitude E_{0+} is small below this threshold due the fact that the $\pi^0 p$ scattering length $a(\pi^0 p)$ is small. Above the $p(\gamma, \pi^+)n$ threshold the imaginary part of E_{0+} is dominated by the two step reaction $\gamma p \rightarrow \pi^+ n \rightarrow \pi^0 p$. The reason this is so large is that $E_{0+}(\gamma p \rightarrow \pi^+ n)$ is over 10 times larger in magnitude then $E_{0+}(\gamma p \rightarrow \pi^0 p)$. Therefore a measurement of the phase of

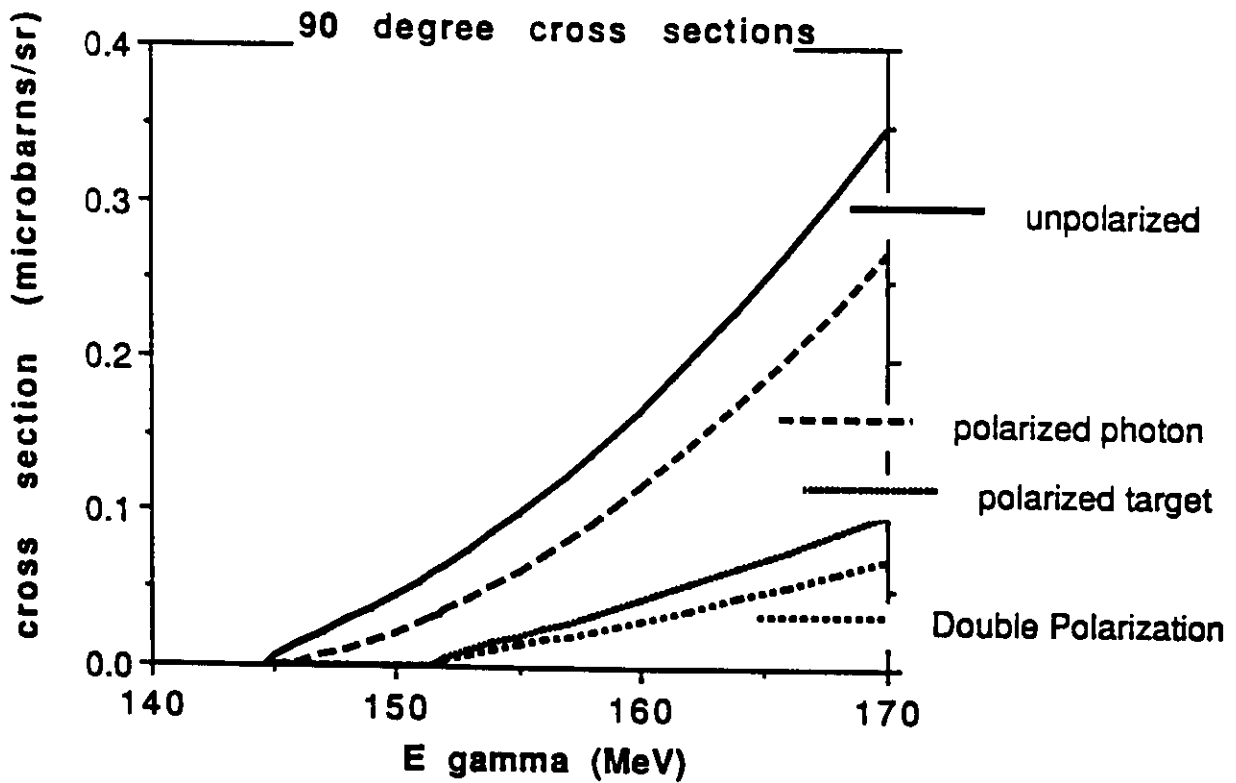


Figure 6: The cross sections including polarization for the $p(\gamma, \pi^0)$ reaction at a pion CM angle of 90° (where the polarization cross sections have maxima). These were calculated with empirical multipoles.[23]

$E_{0+}(\gamma p \rightarrow \pi^0 p)$ in the region above the $p(\gamma, \pi^+)n$ threshold is a measurement of the $\pi^+n \rightarrow \pi^0 p$ charge exchange reaction [see ref. [12], Appendix A].

At the present time the only direct measurement of πN scattering lengths in the low energy region is the level shift for $\pi - p$ atoms.[30] All other measures come from a dispersion theory fit to a global set of pp scattering data starting at ~ 30 MeV kinetic energy and covering the delta region. The inferred scattering lengths are obtained as low energy constants in the dispersion integrals.[24] The latest results of these analyses indicate the systematic dependence on the value of $g_{\pi N}$ (the πN coupling constant). A direct measure the πN scattering length would be of great importance to test the predictions of chiral dynamics.[1, 4, 13] This must be done by the measurement of πN scattering at kinetic energies ~ 10 to 20 MeV in order to avoid the much stronger p-wave effects of the Δ resonance. With the exception of experiments with stopping π^- mesons the experiment proposed here[12] is the only direct way to perform these measurements. It should be noted that if these measurements can achieve sufficient precision, then they can test the predictions of isospin breaking in πN scattering[4] due to the mass difference of the up and down quarks.[4, 8] A very interesting (and easily measured) effect due to isospin breaking dynamics is the variation with energy of the target spin-dependent responses $P(\theta_\pi^*)$ and $H(\theta_\pi^*)$ shown in fig. 3. This is due in part to the difference in threshold energies for the $p(\gamma, \pi^0)p$ and $p(\gamma, \pi^+)n$ reactions, approximately half of which is due to the mass difference of the up and down quarks.

4 The $H(\vec{\gamma}, \pi^0)$ Experiment

The experiment proposed here involves an intense polarized γ beam incident on a dense hydrogen target with the energy and momentum of the produced π^0 's being determined by measurements of the energy and angle of their decay γ 's. The required experimental apparatus development can be divided into four parts:

1. Compton $\vec{\gamma}$ source,

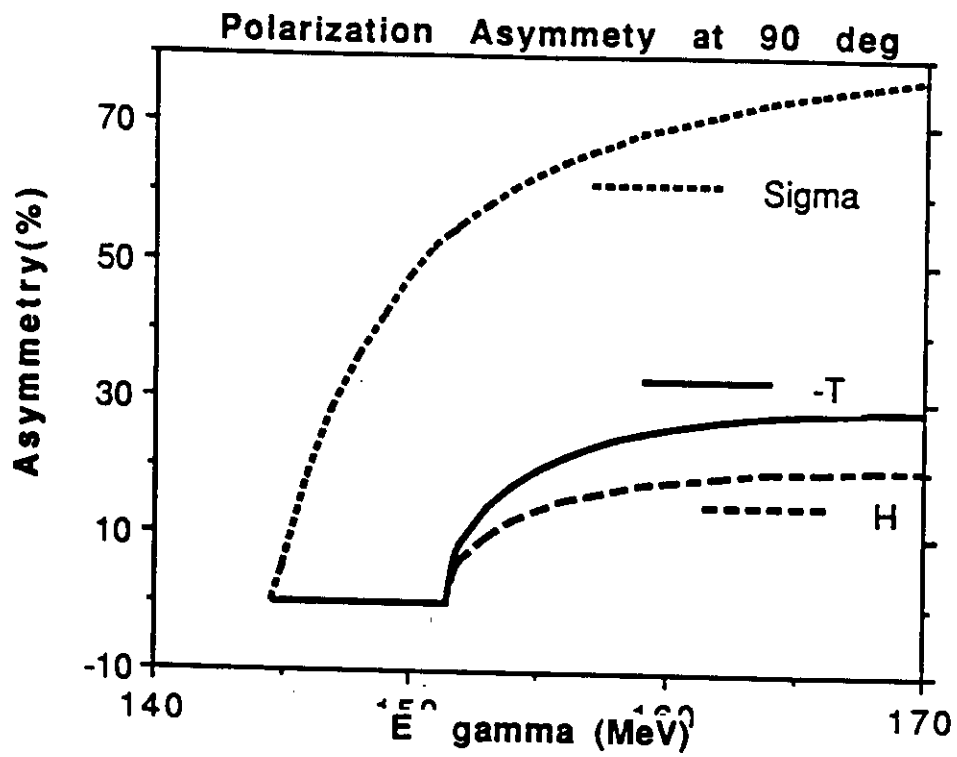


Figure 7: The polarization asymmetries (in %) for $p(\gamma, \pi^0)$ reaction at a pion CM angle of 90° calculated with empirical multipoles.[23] The maximum values for the asymmetries are larger at smaller angles.

2. Tagging spectrometer detector modifications,
3. Target, and
4. Detector.

These will be discussed individually below.

4.1 Compton Polarized Photon Source

The use of Compton scattering of visible light from high energy electrons as a means of producing high energy, polarized photons was first suggested in 1962 by R. Milburn[31] and by F. R. Arutyunian *et al.*[32] Since then the technique has been employed at many laboratories: CEA,[33] the Lebedev Institute,[34] SLAC,[35] and Brookhaven (LEGS).[36, 37] Accordingly, the basic theory and practice are well established.

The principal advantages of this technique over others for producing polarized photons are:

- **Polarization:** The degree of polarization in the uppermost 20% of the spectrum exceeds 90% for linearly polarized photons.
- **Systematic Uncertainties:** The γ polarization is given by the product of the laser photon polarization and a smoothly varying function of the γ energy. The laser polarization is extremely stable in time and, moreover, can be monitored on-line. The smooth dependence on γ energy further reduces possible systematic uncertainties. Finally, the polarization of the laser (and hence the γ beam) is easily and quickly rotated with *no change in the geometry of either the electron or γ beam*. The direction of linear polarization can be varied smoothly and easily over the entire range, thus reducing significantly systematic uncertainties arising from other components of the experimental system.
- **Photon Flux:** With a conservative laser system tagging rates of approximately 1 MHz/MeV can be achieved.

- **Tagging Efficiency:** The kinematics of Compton scattering place a firm upper limit on the energies of the γ 's produced. Accordingly, there are no untagged high energy γ 's. The tight correlation between the γ energy and γ emission angle means that a collimator limiting the γ angle places a lower limit on the energy of transmitted γ 's. Thus, a suitable choice of collimator size can ensure that only γ 's scattered from electrons having energies within the range of interest.
- **Backgrounds:** There is no material target in the path of the electron beam so the principal sources of backgrounds associated with tagged photon beams are essentially eliminated.

The only serious limitation to this technique is that the maximum energy of the γ 's produced is significantly less than that of the electron beam. However, it must be noted that alternative techniques for producing linearly polarized γ 's are similarly limited.

In the following discussions we have, except where noted, assumed a laser photon energy (E_{laser}) of 2.4 eV (corresponding to the 514 nm green line in a standard Ar-ion laser), an electron beam energy (E_{beam}) of 2.3 GeV, and a maximum electron beam power of 20 kW.

When a photon of energy E_{laser} collides head on with an electron of energy E_{beam} and is scattered backwards, emerging at an angle θ_γ with respect to the incident electron energy, its energy is given by

$$E_\gamma = \frac{E_{laser} (E_{beam} + P_{beam})}{E_{beam} + E_{laser} - (P_{beam} - E_{laser}) \cos \theta_\gamma} \quad (8)$$

$$\approx \frac{4\gamma^2 a E_{laser}}{[1 + a(\gamma\theta_\gamma)^2]} \quad (9)$$

where

$$a = \left[1 + \frac{4\gamma E_{laser}}{m_e} \right]^{-1},$$

$$\gamma = E_{beam}/m_e, \text{ and}$$

$$m_e = \text{electron rest mass.}$$

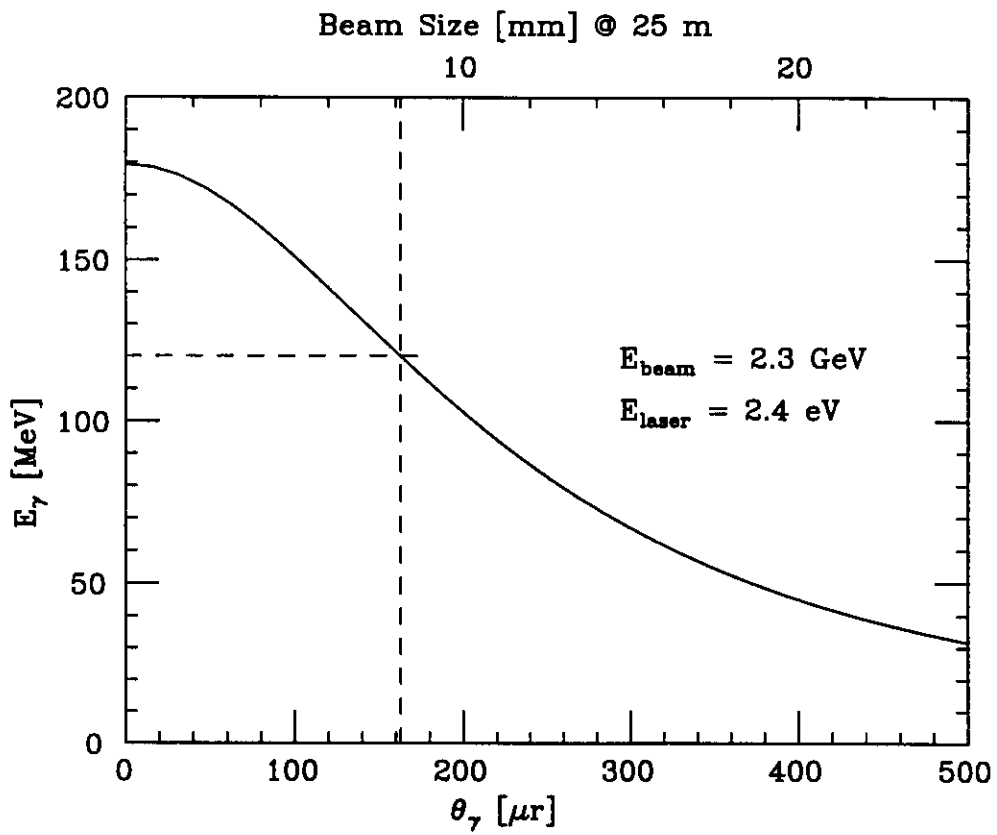


Figure 8: The γ energy is dependent on the laboratory scattering angle with respect to the electron direction.

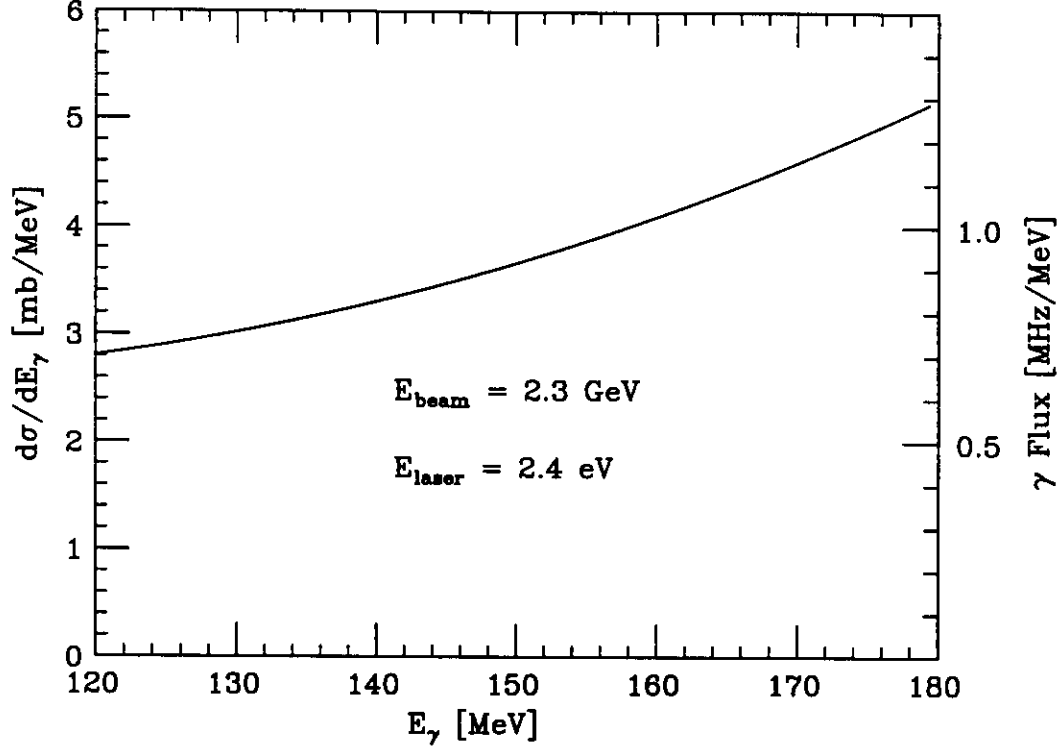


Figure 9: Differential cross section as a function of γ energy.

The relationship for the parameters of interest here is shown in fig. 8.

The cross section for Compton scattering is given (in the laboratory frame) by

$$\frac{d\sigma}{dE_\gamma} = \frac{2\pi r_e^2 a}{E_\gamma^{max}} \left(\frac{\rho^2 (1-a)^2}{1-\rho(1-a)} + 1 + \left[\frac{1-\rho(1+a)}{1-\rho(1-a)} \right]^2 \right) \quad (10)$$

where r_e is the classical radius of the electron ($= 2.818 \text{ fm}$) and $\rho = E_\gamma/E_\gamma^{max}$. The energy spectrum of a γ beam transmitted by an 8 mm collimator placed 25 m from the laser-electron interaction point is shown in fig. 9.

The linear polarization of the γ beam (P^γ) relative to that of the laser beam (P^{laser}) is given by

$$\left| \frac{P^\gamma}{P^{laser}} \right| = \frac{(1 - \cos \theta_0)^2}{2 [\kappa + 1 + \cos \theta_0^2]} \quad (11)$$

where

$$\begin{aligned} \kappa &= \frac{\rho^2 (1 - a)^2}{1 - \rho(1 - a)} \text{ and} \\ \cos \theta_0 &= \frac{1 - \rho(1 + a)}{1 - \rho(1 - a)} \end{aligned}$$

and is shown in figure 10.

In order to obtain a reasonable flux of tagged γ 's using an electron beam current of the order of μA 's it is necessary to obtain a very high incident photon flux. The proposed means of achieving such a high flux is a Fabry-Perot resonant cavity[38] in which the photons from a laser are stored. In one sense, the proposed system is the mirror image of the LEGS system. At LEGS, photons of a relatively low intensity laser beam interact once with a high intensity electron beam (achieved by storing in a ring). At CEBAF, electrons of a relatively low intensity electron beam will interact once with a high intensity photon beam (achieved by storing in a resonant cavity).

A Letter-of-Intent (LOI) for the construction of this facility was submitted to PAC-6.[39] The design presented in the LOI has since been refined principally to facilitate its inclusion into the electron beam line into Hall B. Originally, it was planned to introduce a vertical displacement of the electron beam and to place a linear Fabry-Perot cavity such that the photon beam and the displaced electron beam were colinear for a distance of approximately 4 m. The $\tilde{\gamma}$ beam would then be emitted parallel to but displaced from the electron beam [see fig. 11(a)]. It was subsequently determined that using a "figure 8" cavity with tightened focussing at the cross-over point gave similar $\tilde{\gamma}$ fluxes when the electron beam, with similarly tightened focussing, intersected the cavity at the cross-over point [see fig. 11(b)].

The modified design has four distinct advantages:

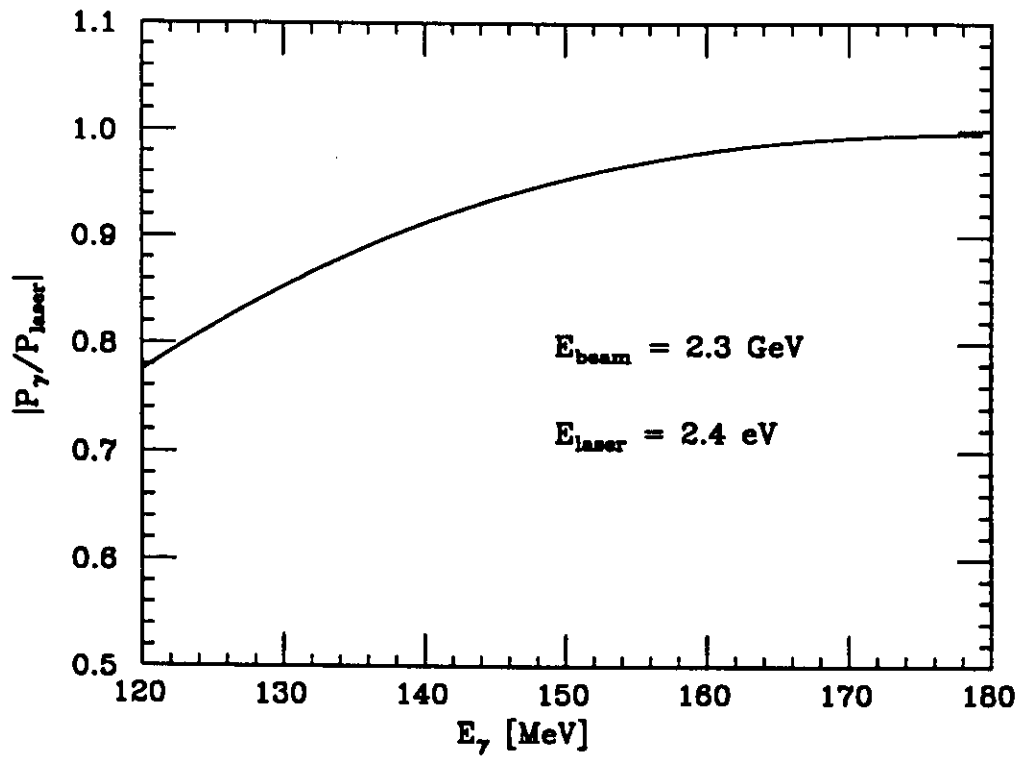


Figure 10: Backscattered γ polarization as a fraction of the incident laser polarization.

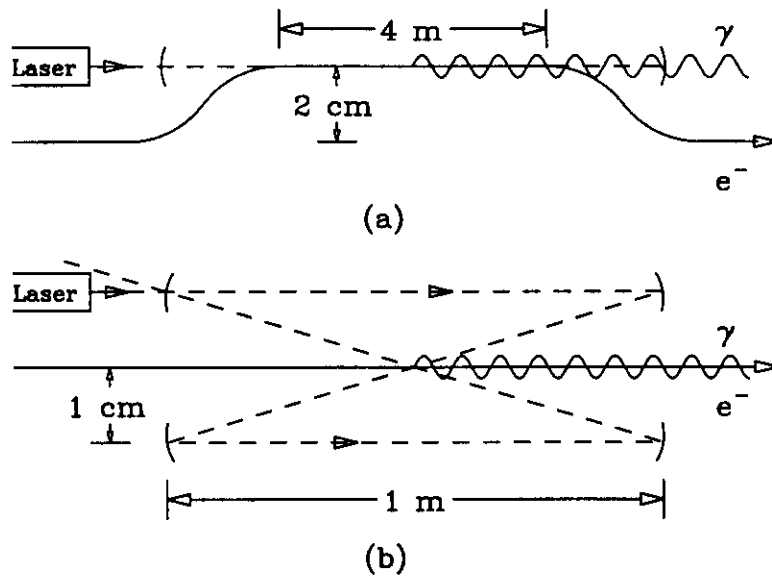


Figure 11: Schematic layout of proposed Compton $\vec{\gamma}$ source. (a) Layout as presented in ref. [39]. (b) Layout as currently envisaged.

1. No changes are required in the electron beam line.
2. $\vec{\gamma}$'s are emitted colinear with the nominal electron beam axis. No modifications to either the beam pipe or the entrance end of the tagger vacuum box are required.
3. The mirrors comprising the optical cavity can be shielded from synchrotron radiation.
4. Laser light reflected from the input coupling mirror to the cavity (primarily during emptying and filling when the polarization direction is changed) is not directed towards the laser.

The anticipated $\vec{\gamma}$ fluxes for the proposed experiment (see fig. 9) were calculated using the new geometry, a cavity length of 2 m, a crossing angle (θ_c) of 20 mr, a single frequency laser power of 10 W, $g = -0.95$ [38], a cavity gain of 30,000 (based on mirrors with Transmission+Absorption+Scattering of a few parts per million), an electron beam emittance of 10^{-9} m-radians, and electron β -functions of about 1 m. None of these values exceeds current state-of-the-art limits.

4.2 Tagging Spectrometer

The tagging spectrometer detector package, as currently designed, will detect electrons with between 5% and 80% of the incident beam energy corresponding to γ 's with energies between 20% and 95% of the incident electron beam energy. In the proposed experiment γ 's with energies between 120 MeV and 180 MeV will be produced from a 2.3 GeV electron beam. Accordingly, electrons with energies between 92% and 95% of the initial electron beam energy must be detected. These electrons will not only miss the currently planned detectors but will also exit the tagging spectrometer magnet through a roughly perpendicular field boundary and will experience no first order focussing. Thus, for the present purposes the tagging spectrometer magnet can be regarded as a simple non-focussing dipole spectrometer.

The dispersion (D) generated by a dipole field is given by:

$$D = \langle x|\delta \rangle = \rho_0 (1 - \cos \theta_0) \quad (12)$$

where ρ_0 is the nominal bending radius and θ_0 is the nominal bending angle. For the Hall B tagging spectrometer magnet $D = 1.7$ cm/%. Similarly, the angular dispersion (D') is given by:

$$D' = \langle \theta|\delta \rangle = -\sin \theta_0. \quad (13)$$

For the Hall B tagging spectrometer magnet $D' = 5$ mr/%. Therefore, the dispersion at a detector placed 3 m from the exit face of the tagging spectrometer magnet will be about 3 cm/%. A goal for the resolution of 3×10^{-4} or 500 KeV implies that the achromatic size of the beam at the detector be not greater than about 100 μm .

At this point it must be noted that in the Compton scattering process the electrons are deflected by at most 9 μr . At the point of scatter the electron β -function is about 1 m, corresponding to a divergence of about 30 μr in an $\epsilon_{\perp} = 10^{-9}$ m-r beam. The additional divergence due to the scattering represents a negligible (<2%) effective increase in the beam emittance. Achieving an achromatic spot size of 100 μm therefore simply requires tuning the beam at the entrance to the tagging spectrometer magnet. For example, a β -function of 25 m and an α -function of about 6 at the magnet entrance would satisfy this requirement. Essentially, we will use quadrupoles in the beam line to convert the single dipole tagging spectrometer into a QD or QQD configuration with an exceedingly small solid angle acceptance. The details of this tuning have not been finalized. This will be done in conjunction with the overall design of the Hall B beam line.

The tagging spectrometer detector for the proposed experiment must have a position resolution of at most 100 μm and be able to handle rates of 50 MHz across the full acceptance or about 50 kHz per channel. Several options are under consideration but no decision has been made. A most promising option is to use scintillating fibers.

The length of the detector required to detect all electrons corresponding to photons in the energy range to be accepted by the collimator is less than

10 cm if it is placed perpendicular to the electron trajectories, less than 15 cm if it is placed at an angle of 45° . Accordingly, this detector will be of a size appropriate for a prototype of a detector suitable for use when the energy range of the Compton $\vec{\gamma}$ source is extended through the use of higher electron energies and/or shorter laser wavelengths.

4.3 Target

In the initial phase of our study of the $p(\gamma, \pi^0)p$ reaction proposed here we plan to use a liquid H_2 target. It will have a diameter of slightly more than 1 cm and a length of 2 cm. No special requirements are placed on this target. The cryogenic target currently being prepared for general use with the CLAS will, with minor modifications, be suitable for use in this experiment.

4.4 Detector

The detector to be used in the proposed experiment is currently under construction at PSI. It was originally designed at the University of Virginia for use in a measurement of the $\pi^+ \rightarrow \pi^0 e^+ \nu$ decay rate at PSI and a detailed description can be found in ref. [40]. Inasmuch as the detection of π^0 decays is a crucial component of that experiment this detector is almost ideally suited to our purposes. Schematically (see fig. 12), the detector consists of a) two wire chambers surrounding the target, b) thin scintillator veto detectors, and c) a geodesic ball of ultrapure CsI blocks comprising a shower counter for the detection of the decay γ 's.

The detector components nearest the target are the charged particle tracking detectors which consist of two cylindrical wire chambers, each with one anode wire plane in the beam direction and two cathode strips in stereoscopic geometry. The design of these chambers parallels that of the CP-LEAR PC2 chambers[41]; their principal parameters are listed in table 2. It is not clear that these chambers will be required for the proposed experiment.

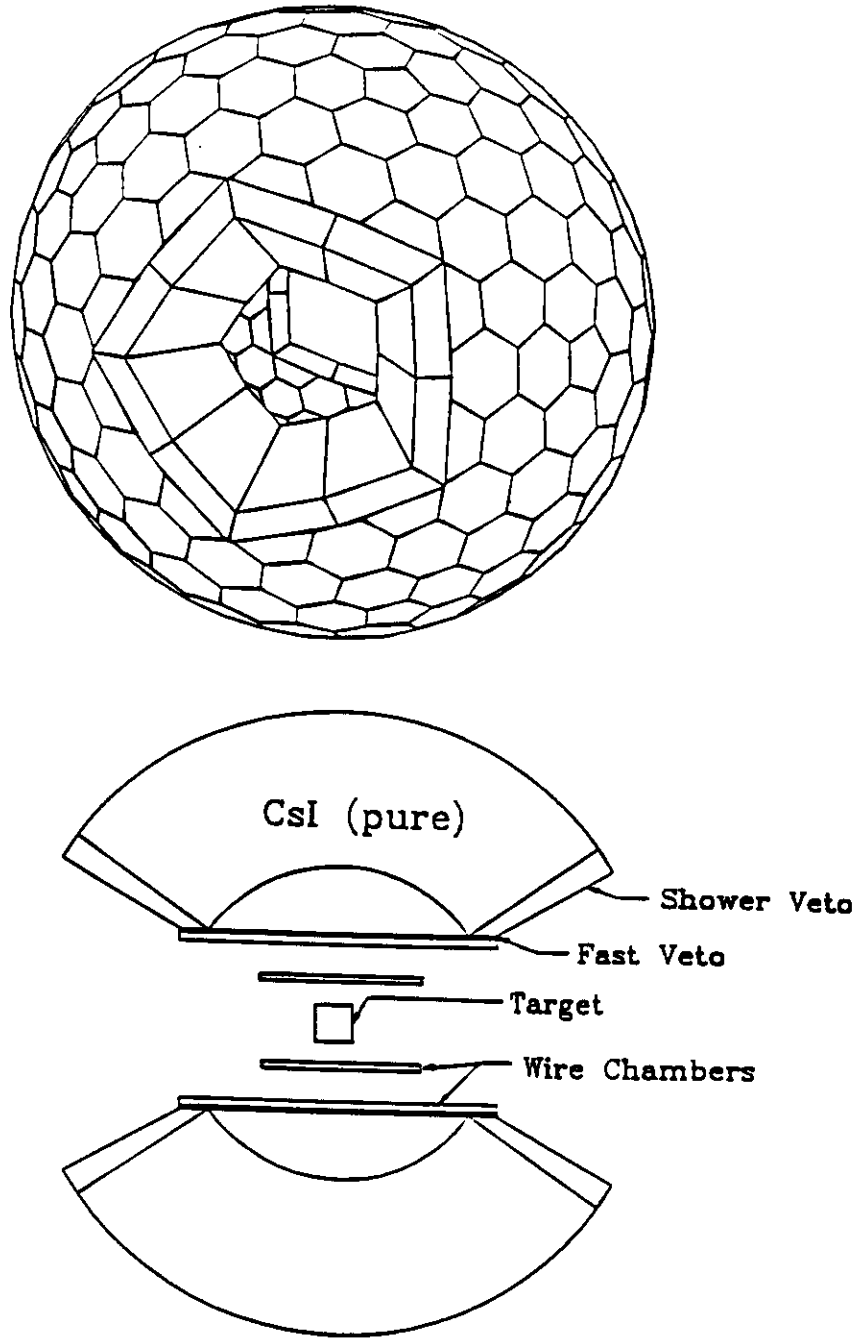


Figure 12: UVA/PSI detector

The next layer of detectors consists of fast veto counters constructed from plastic scintillator. The principal purpose of these detectors is to veto charged particles coming from the target. Based upon past experience and Monte Carlo simulations with the GEANT code these detectors are expected to be >90% efficient. The principal parameters of these detectors are listed in table 3.

The heart of the detector package is the CsI shower calorimeter. It consists of 225 blocks of ultra pure CsI arranged in a nearly spherical geometry obtained by the geodesic triangulation of an icosahedron; in this respect it is similar to the SLAC Crystal Ball.[42] However, the PSI/UVA detector consists of truncated hexagonal and pentagonal pyramids rather than the triangular pyramids of the Crystal Ball since this configuration has superior light collection efficiency. The principal parameters of the shower detector geometry are listed in table 4.

The granularity of this detector was chosen such that 90% of the shower caused by a photon striking the center of a block will be contained within that block. At most three modules will share significant portions of a single particle's showered energy. This sharing of the energy among blocks permits a reconstruction precision that is significantly smaller than that corresponding to the solid angle subtended by a single block.

5 Simulations

In modelling the proposed experiment we included the following component properties and effects:

- Polarized γ beam (see Sec. 4.1) - electron beam energy spread and emittance, laser beam size and divergence, resultant $\vec{\gamma}$ divergence;
- Tagger (see Sec. 4.2) - detector size;
- Target (see Sec. 4.3) - realistic geometry, cell walls, contaminants;

- CsI Detector (see Sec. 4.4) - finite resolution effects, including energy spread, and spatial resolution.

The possible production of a π^0 was identified by the simultaneous detection in the CsI detector of two γ 's in coincidence with the detection in the tagger detector of an electron. The π^0 energy was determined using the "X-formula,"

$$E_\pi = \frac{2m_\pi^2}{(1 - X^2)(1 - \cos \phi)}$$

$$X = \frac{E_1 - E_2}{E_1 + E_2}$$

where E_π is the total π^0 energy, m_π is the π^0 mass, E_1 and E_2 are the energies of the two decay γ 's, and ϕ is the opening angle between the π^0 decay γ 's. The direction of the π^0 was similarly determined using the γ energies and emission angles. A missing mass spectrum for the undetected reaction product(s) was then computed.

Background contributions to the π^0 spectrum come from two principal sources: quasifree production from contaminant nuclei or nuclei in the target cell walls and coherent production from these nuclei. Contributions from quasifree production were computed using Fermi gas models of the nuclei and on-shell production amplitudes. Contributions from coherent production were computed using a parameterization of the measured cross sections. Background events arising from the accidentally coincident detection of two γ 's from independent sources are almost totally absent. This is a direct consequence of the facts that a) the tagging efficiency of a Compton $\vec{\gamma}$ source is very nearly 100% and b) there is essentially no background radiation generated by the source, in contrast to the case when Bremsstrahlung production is employed. Figure 5 shows the simulated missing mass spectrum wherein the absence of a background is evident.

The precision with which the simulations indicate we can determine observables and amplitudes derived therefrom is presented in Section 6 where the request for beam time is discussed.

Figure 13: Simulated missing mass spectrum. The abscissa shows the reconstructed missing mass in units of the proton mass. The ordinate shows the number of simulated events. Note that the width of the distribution is less than 1 nucleonic mass and the level of background is negligible.

6 Beam Time Request

The total beam time requested for this experiment is 400 hours. This time was determined using the following assumptions:

1. A working Compton $\bar{\gamma}$ source (see Sec. 4.1) with $\bar{\gamma}$ energies ranging from 120 MeV to 180 MeV.
2. Tagging resolution corresponding to a γ energy resolution of 500 keV (see Sec. 4.2).
3. Tagged γ rates of 1 MHz per MeV.
4. A 2 cm long liquid hydrogen target (see Sec. 4.2).
5. The University of Virginia CsI crystal ball with polar coverage from 30 degrees to 170 degrees and full azimuthal coverage (see Sec. 4.4).

Using the experimentally measured π^0 production cross section from Mainz[15] at $E_\gamma = 154$ MeV and the above assumptions we estimate a counting rate of 200 detected π^0 's per hour. Our simulations indicate that a reconstruction efficiency of $\sim 50\%$ represents a conservative estimate so we expect 100 reconstructed π^0 's per hour. Table 5 lists the expected number of events and statistical uncertainties for various observables over a range of final state energies. In estimating the running time required (see table 8) we assumed a macroscopic duty factor of 75%. For the asymmetry due to γ polarization we assumed a value computed using Chiral perturbation theory since this theory yields the smallest asymmetries and therefore generates the most conservative estimate.

To extract the multipole amplitudes we used a fitting procedure over the different γ energies and angular distributions. The expected statistical uncertainties in the extracted multipole amplitudes are presented in table 7.

Table 8 lists the beam-on-target time required for this experiment. We will also require approximately 10 days of access time to set up, and about 3 days to take down the experimental apparatus.

Table 2: Principal parameters of the charged particle tracking detectors.

Parameter	Inner	Outer
Active Length [mm]	350	540
Inner radius [mm]	42.5	107.5
Wire layer radius [mm]	60	120
Outer radius [mm]	70	128
# of wires	192	384
Cathode strip width [mm]	$\cong 3$	2
# Number of strips	256	448
Gas half gap [mm]	2.5	2.5
Chamber wall thickness [rad. len.]	0.0013	0.0019

Table 3: Principal parameters of the plastic scintillator fast veto detectors.

Parameter	
Outer radius [mm]	140
Active length [mm]	550
Thickness [mm]	5
Number of modules	20 (interleaved edges)
Readout	longitudinal, both ends, PMT's

Table 4: Principal parameters of the CsI shower calorimeter.

Parameter	
Inner radius [mm]	260
Outer radius [mm]	480
Average thickness [rad. len.]	12
# of modules	225
# of active modules	195
# of edge veto modules	30
Total solid angle	$\cong 0.77$ of 4π sr
Average solid angle per module	$0.004 \times 4\pi$ sr
Geodesic breakdown	Class II
Volume of CsI	$\cong 346,000$ cm ³
Expected optical nonuniformity	< 2.5% FWHM
Readout	50 mm PMT's with quartz windows

Table 5: Expected statistical uncertainties in the total cross sections (σ), the differential cross sections ($d\sigma$), and the asymmetries due to γ polarization ($d\Sigma$).

$E_\gamma - E_\gamma^{thres}$ [MeV]	N_π^{total}	$\frac{\delta\sigma}{\sigma}$	$\frac{\delta d\sigma}{d\sigma}$	$\frac{\delta d\Sigma}{d\Sigma}$
1	1,800	2.4%	3.0%	25%
3	5,200	1.4%	2.3%	18%
5	8,800	1.1%	1.8%	13%
π_{thres}^+	9,800	1.0%	1.4%	9%
9	13,200	0.9%	1.2%	7%

Table 6: Expected statistical uncertainties in the extracted multipole amplitudes.

Multipole	Uncertainty
$ E_{0+} $	5%
$ E_{1+} $	8%
$ M_{1+} $	2%
$ M_{1-} $	8%

Table 7: Requested beam time for this experiment.

Description	Energy	Current	Shifts
Detector tune up	2.3 GeV	1 μ A	5
$\bar{\gamma}$ source tune up	2.3 GeV	4-5 μ A	2
Identification of systematic errors	2.3 GeV	4-5 μ A	3
Energy calibration using CH ₂	2.3 GeV	4-5 μ A	3
Actual measurement	2.3 GeV	4-5 μ A	37
Total			50

References

- [1] E. Amaldi, S. Fubini, and G. Furlan, *Pion-Electroproduction*, Vol. 83 of *Springer Tracts in Modern Physics* (Springer-Verlag, New York, 1979),
- [2] J. F. Donoghue, E. Golowich, and B. R. Holstein, *Dynamics of the Standard Model* (Cambridge University Press, Cambridge, 1992).
- [3] S. Weinberg, *Phys. Rev. Lett.* **17**, 168 (1966).
- [4] S. L. Adler and R. F. Dashen, *Current Algebra and Applications to Particle Physics* (Benjamin, NEW YORK, 1968).
- [5] P. de Baenst, *Nucl. Phys.* **B24**, 633 (1970).
- [6] U. G. Meißner, *Rep. Prog. Phys.* **56**, 903 (1993).
- [7] J. Gasser and H. Leutwyler, *Annals of Physics* **158**, 142 (1984).
- [8] J. Gasser and H. Leutwyler, *Phys. Rep.* **87**, 77 (1992).
- [9] S. Weinberg, *Trans. N. Y. Acad. Sci., Ser. II* **3**, 185 (1977).
- [10] V. Bernard, N. Kaiser, and U. G. Meißner, *Nucl. Phys.* **B383**, 442 (1992).
- [11] V. Bernard, N. Kaiser, T. S. H. Lee, and U. Meißner, *Phys. Rev. Lett.* **70**, 387 (1993), and to be published.
- [12] A. Bernstein, to be published; included as Appendix 1.
- [13] V. Bernard, N. Kaiser, and U. G. Meißner, *Phys. Lett.* **B309**, 421 (1992).
- [14] E. Mazzucato *et al.*, *Phys. Rev. Lett.* **57**, 3144 (1986).
- [15] R. Beck *et al.*, *Phys. Rev. Lett.* **65**, 1841 (1990).
- [16] A. M. Bernstein and B. R. Holstein, *Comments on Nuclear and Particle Physics* **20**, 197 (1991).
- [17] J. Bergstrom, *Phys. Rev. C* **44**, 1768 (1991).

- [18] H. W. L. Naus, J. H. Koch, and J. L. Friar, *Phys. Rev. D* **41**, 2852 (1990).
- [19] H. W. L. Naus, *Phys. Rev. C* **43**, R365 (1991).
- [20] J. P. Burq, *Annals of Physics* **10**, 363 (1965).
- [21] M. J. Adomovitch *et al.*, *Sov. J. Nucl. Phys.* **2**, 95 (1966).
- [22] E. L. Goldwasser *et al.*, in *Proc. XIII International Conf. High Energy Physics*, edited by Y.-A. Smorodinsky (USSR Academy of Sciences, Dubna, USSR, 1964).
- [23] E. Guillian, B.S. Thesis, 1992.
- [24] D. Drechsel and L. Tiator, *J. Phys. G***18**, 449 (1992).
- [25] S. Nozawa, T. S. H. Lee, and B. Blankleider, *Phys. Rev. C* **41**, 213 (1990).
- [26] 1992, tAPS Experiment at Mainz, H. Stroher, spokesman.
- [27] A. S. Raskin and T. W. Donnelly, *Annals of Physics* **191**, 78 (1989).
- [28] I. S. Barker, A. Donnachie, and J. K. Storrow, *Nucl. Phys. B***95**, 347 (1975).
- [29] G. Hohler, *Pion Nucleon Scattering* **9b**, 1 (1983).
- [30] W. Beer *et al.*, *Phys. Lett. B***261**, 16 (1991).
- [31] R. H. Milburn, *Phys. Rev. Lett.* **10**, 75 (1963).
- [32] F. R. Arutyunian, I. I. Goldman, V. A. Tumanian, and Z. Eksperim, *Soviet Physics, JETP* **18**, 1964 (1964).
- [33] C. Bentspoad, R. H. Milburn, N. Tanaka, and M. Fotino, *Phys. Rev. B* **138**, 1548 (1965).
- [34] O. F. Kulikov, Y. Y. Telnov, E. I. Filippov, and M. N. Yakimenko, *Phys. Lett.* **13**, 344 (1964).

- [35] J. J. Murray and P. R. Klein, SLAC-TN-67-19 **19**, 1 (1967).
- [36] A. M. Sandorfi *et al.*, IEEE NS-**30**, 3083 (1983).
- [37] C. E. Thorn *et al.*, Nucl. Instrum. Meth. A**285**, 447 (1989).
- [38] A. E. Siegman, *An Introduction to Lasers and Masers* (McGraw-Hill, New York, 1971).
- [39] B. E. Norum and T. P. Welch, An Intense Polarized Photon Source at CEBAF Hall B, 1993, letter-of-Intent LOI-93-012 submitted to CEBAF PAC-6.
- [40] D. Počanić *et al.*, A Precise Measurement of the $\pi^+ \rightarrow \pi^0 e^+ \nu$ Decay Rate, a proposal for an experiment at PSI, 1992.
- [41] P. R. Kettle, private communication, 1990.
- [42] M. Oreglia *et al.*, Phys. Rev. D **25**, 2259 (1982).
- [43] C. G. Fasano, F. Tabakin, and B. Saghai, Phys. Rev. C **46**, 2430 (1992).
- [44] G. Anton, J. Arends, W. Beulertz, and J. Hey, Nucl. Instrum. Meth. A **310**, 631 (1991).

Appendices

A New Tests of Chiral Dynamics

Following is a preprint of a paper titled "A New Method To Measure Low Energy πN Interactions: Tests of Chiral Dynamics" by A. Bernstein.

A New Method To Measure Low Energy πN Interactions: Tests of Chiral Dynamics

A. M. Bernstein

Physics Department and Laboratory for Nuclear Science

Massachusetts Institute of Technology

Cambridge, MA USA

(April 24, 1994)

Abstract

A new method is proposed to measure πN interactions at low energies and in previously inaccessible combinations of charge states by observing the phase of the near threshold amplitudes for the $\gamma N \rightarrow \pi N$ reactions. From unitarity and time reversal invariance the phase of the photo (electro) production amplitudes are related to the hadronic phase shifts in the final state (generalization of the Fermi-Watson theorem). New experimental facilities and techniques make phase measurements feasible. This can be used to test isospin invariance, the predictions of chiral perturbation theory for the πN scattering lengths, and to constrain the empirical value of the πN sigma term.

Low energy πN interactions are of fundamental interest since they can be predicted by soft pion theorems [1,2] which are now believed to represent approximations to QCD by the use of chiral perturbation theory [3]. Experimental requirements restrict what measurements can be made since low energy charged pion beams and π^0 beams (at any energy) cannot be made. Because of nuclear structure uncertainties interactions involving neutrons can be difficult to measure accurately. Measurements of the $\pi^0 p$ and $\pi^+ n$ phase shifts and the $\pi^+ n \rightarrow \pi^0 p$ charge exchange amplitude can be made by the observation of the final state interactions in photo (electro) production. Experiments in previously inaccessible charge state combinations can be used to study the predicted violation of isobaric invariance of πN interactions due to the mass difference of the up and down quarks [4].

Using soft pion (PCAC) techniques the s wave πN scattering lengths were predicted [1] to be $a_{1/2} = m_\pi/4\pi F_\pi^2 = 0.175/m_\pi$ and $a_{3/2} = -a_{1/2}/2 = -0.088/m_\pi$, where $I = 1/2, 3/2$ is the isospin of the πN system and $F_\pi \cong 93$ MeV is the pion decay constant. These predictions are not easy to test since πN scattering experiments have not been performed at kinetic energies below ~ 30 MeV. This means that the s and p wave contributions to the cross sections are of the same magnitude and the s wave scattering lengths must be obtained from low energy extrapolations of global fits to the data [5]. The extracted values of $a_{1/2} = 0.173(3)/m_\pi$ and $a_{3/2} = -0.101(4)/m_\pi$ [5] are in reasonable agreement with the soft pion predictions [1]. The quoted errors are too small since they only take internal inconsistencies of the method into account and not the fact that the πN scattering data are not internally consistent [6]. The best low energy test for the scattering lengths comes from the measurement of the strong interaction shift in the $\pi^- p$ atoms and gives $a(\pi^- p) = [2a_{1/2} + a_{3/2}]/3 = 0.086(0.004)/m_\pi$ [7] in good agreement with the soft pion prediction of $0.087/m_\pi$.

For the $\pi^0 N$ scattering $a(\pi^0 p) = a(\pi^0 n) = [a_{1/2} + 2a_{3/2}]/3 \cong 0$; [1] this null result means that $\pi^0 N$ interactions are particularly sensitive to the underlying dynamics. Later, using a chiral Lagrangian Weinberg [4] showed that $a(\pi^0 N) = a_B + a_\sigma$

$$\begin{aligned}
a_B &= -g_A^2 m_\pi^2 / [16\pi(M + m_\pi)F_\pi^2] = -8.91 \times 10^{-3} / m_\pi \\
a_\sigma &= M\sigma / [4\pi(M + m_\pi)F_\pi^2] \\
\sigma &= \langle m_u \bar{u}u + m_d \bar{d}d \rangle
\end{aligned} \tag{1}$$

where σ is the πN sigma term [3,8] and a_B is a Born term. Inserting the estimates of the quark masses [4,9] or using the value of the σ term [8] in Eq. 1 we obtain $0.010/m_\pi \leq a(\pi^0 p) \leq 0.037/m_\pi$. As a consequence of the mass difference of the up and down quarks [4,9] $a(\pi^0 n) - a(\pi^0 p) \cong 0.004/m_\pi$. The prediction of an isospin violation in the low energy πN interactions is important to test experimentally.

The corrections to the πN scattering lengths have recently been calculated using chiral perturbation theory [10]; in addition to the lowest order terms [1] and the two terms of Eq. 1 [4] several other contributions were found. For charged pion scattering the corrections to the soft pion results [1] are small. For $\pi^0 N$ scattering the magnitude of the corrections are more uncertain since they depend on several unknown parameters [10].

In this paper it is shown (for the first time) that the phase shifts for low energy πN scattering can be obtained from the final state interaction in photo (electro) pion production by a phase measurement of the near threshold amplitudes. The relationship between the phase of the multipole amplitude and the phase shift in the final state was derived by Fermi and Watson [11]. It is based on unitarity, time reversal invariance, and on the weakness of the electromagnetic compared to the strong interaction which was assumed to include isospin conservation. For photo (electro) pion production from the proton there are three channels, γp , $\pi^0 p$, and $\pi^+ n$. By assuming isospin conservation the problem is reduced to two channels. However, isospin symmetry is badly broken in the threshold region due to Coulomb effects and different up and down quark masses which lead to different threshold energies for the $\pi^0 p$ and $\pi^+ n$ channels. Therefore the Fermi-Watson theorem cannot be applied; to handle this problem it is generalized by dropping the requirement of isospin conservation and working with the charge states. The S matrix can be written as [12]:

$$S = \begin{pmatrix} S_\gamma & iM_0 & i\theta M_+ \\ iM_0 & S_0 & \theta S_{0+} \\ i\theta M_+ & \theta S_{0+} & \theta S_+ \end{pmatrix} \quad (2)$$

Where $S_0 = \cos \phi e^{2i\delta_0}$, $S_+ = \cos \phi e^{2i\delta_+}$ and $S_\gamma = e^{2i\delta_\gamma}$ represents elastic $\pi^0 p$, and $\pi^+ n$, and γN scattering respectively, δ_0, δ_+ , and δ_γ are their phase shifts, $S_{0+} = i \sin \phi e^{i(\delta_+ + \delta_0)} = S_{+0}$ represents the $\pi^+ n \leftrightarrow \pi^0 p$ charge exchange amplitude, $\phi(W)$ represents the charge exchange phase, $\cos \phi$ represents the inelasticity due to charge exchange, and for convenience the off diagonal matrix elements for the photoproduction of the $\pi^0 p$, and $\pi^+ n$ channels are written as iM_0 and iM_+ , where M_0 and M_+ are proportional to the multipoles for these channels, and $\theta \equiv \theta(W) = 0(1)$ when W the total CM energy is below (above) the $\pi^+ n$ production threshold. Although not explicitly written here all of these quantities are for a fixed value of W and represent a specific quantum state $\alpha = (\ell, j)$, the orbital and total angular momenta respectively. The S matrix is symmetric due to time reversal invariance. The form of the 2×2 πN part of the S matrix has been chosen to be separately unitary and time reversal invariant. Below the $\pi^+ n$ production threshold the S matrix reduces to the two open channels, γp and $\pi^0 p$, and $\phi(W) = 0$.

Unitarity requires that $S^+ S = S S^+ = 1$. Applying this condition, and assuming the weakness of the EM interaction by dropping terms of order e (except for δ_γ) as assumed by Fermi and Watson, one obtains [12]:

$$\begin{aligned} M_0 &= e^{i(\delta_0 + \delta_\gamma)} [A_0 \cos \phi/2 + i \theta A_+ \sin \phi/2] \\ M_+ &= \theta e^{i(\delta_+ + \delta_\gamma)} [A_+ \cos \phi/2 + i A_0 \sin \phi/2] \end{aligned} \quad (3)$$

where A_0 and A_+ are real functions of the photon energy k . This is as much information as one can extract in terms of the symmetry properties of the S matrix. For the s wave multipoles [13] which we are primarily concerned with here $M_0 = 2\sqrt{q_0 k} E_+$ ($\pi^0 p$) and $M_+ = 2\sqrt{q_+ k} E_{0+}(\pi^+ n)$ where $q_0(q_+)$ are the $\pi^0(\pi^+)$ CM momenta and k is the photon CM energy. The approximate physical interpretation of A_0 and A_+ are the threshold multipoles

in the absence of charge exchange reactions. In Eq. 3 the phase shifts δ and ϕ are divided by two compared to the πN sector because the πN interactions take place in the final state only. Eq. 3 takes δ_γ , the phase shift of elastic photon-nucleon scattering, into account. Using the Compton scattering amplitude [14] in the appropriate channel (f_{EE}^{1-}) it has been shown that δ_γ is negligible (it is only 3% of δ_0 at the π^+n threshold). In Eqs 2 and 3 the unitarity has been calculated to order e (with the exception of δ_γ which is of order e^2). If the unitarity condition is carried out to order e^3 then Eq. 3 (which is of order e) will be modified by terms of order e^3 which is expected to be negligible. This can be checked after the experiments have been performed as has been done for the Compton effect in the Δ region [15].

Eq. 3 is valid for both photo and electroproduction. In the case of electroproduction the amplitudes M_0, M_+, A_0 , and A_+ are functions of q^2 (the invariant four momentum transfer) and W (the total CM energy), whereas the final state interaction parameters δ and ϕ are functions of W only. For photoproduction, $q^2 = 0$ and all of the quantities are functions of W only.

Above the π^+n threshold Eq. 3 shows the close linkage between the open $\pi^0 p$ and π^+n channels. It is helpful to illustrate the quantities in Eq. 3 in the limit of full isospin symmetry, and also to take the limit as the pion CM momentum $q \rightarrow 0$ (threshold). In that case one obtains $\delta_0 = (2 a_{3/2} + a_{1/2})q/3$, $\delta_+ = (a_{3/2} + 2 a_{1/2})q/3$, and $\phi/2 = \delta_{CEX} = \sqrt{2} [a_{1/2} - a_{3/2}]q/3$.

The phases of the threshold multipoles, $\chi(\pi N)$, are obtained from $\tan \chi(\pi N) = Im E_{0+}(\pi N)/Re E_{0+}(\pi N)$ where the real and imaginary parts of $E_{0+}(\pi N)$ are calculated using Eq. 3. Estimates have been made assuming that A_0 and A_+ are the threshold photoproduction s wave amplitudes $E_T(p\pi^0)$ and $E_T(n\pi^+)$ calculated by chiral perturbation theory [10], while the πN phase shifts have been calculated using the predictions [1,4] for the scattering lengths discussed above. To be conservative the smallest value of $a(p\pi^0) \sim 0.010/m_\pi$ was assumed which means that δ_0 could be as much as 4 times larger.

The result for the phase angle $\chi(\pi^0 p)$ is shown in Fig. 1a. Below the π^+n threshold

$\chi(p\pi^0) = \delta_0$ since only one channel is open. It should be pointed out that it is only the energy region between the π^0 and π^+ thresholds where the two channel unitarity is exact.

Above the $n\pi^+$ threshold the phase $\chi(\pi^0 p)$ increases rapidly because it is dominated by the two step charge exchange amplitude $\gamma p \rightarrow \pi^+ n \rightarrow \pi^0 p$. This happens because $E_{0+}(\gamma p \rightarrow \pi^+ n) \gg E_{0+}(\gamma p \rightarrow \pi^0 p)$ and $a_{CEX}(n\pi^+ \rightarrow p\pi^0) \gg a(p\pi^0)$. One MeV above the $\gamma p \rightarrow n\pi^+$ threshold the elastic $\gamma p \rightarrow p\pi^0$ contribution to the phase $\sim 0.2^\circ$ while the dominant two step contribution contributes $\sim 10^\circ$. A measurement of $\chi(\pi^0 p) = \delta_0$ below the $\gamma p \rightarrow n\pi^+$ threshold will allow one to determine $a(p\pi^0)$, a measurement above this threshold will determine $a(n\pi^+ \rightarrow p\pi^0)$. In Fig. 1b, $\chi(\pi^+ n)$, the phase of $E_{0+}(\pi^+ n)$, is shown. The contributions from $\gamma p \rightarrow p\pi^0 \rightarrow n\pi^+$ charge exchange is relatively small, although it is finite at the $n\pi^+$ threshold due to the fact that the $p\pi^0$ channel is already open. Measurement of $\chi(\pi^+ n) \cong \delta_+$ will enable one to obtain $a(n\pi^+)$ for the first time. The dramatic pattern of the phases of the threshold amplitudes E_{0+} predicted here have not yet been measured. They are consequence of isospin symmetry breaking and are due both to electromagnetic effects and to the mass difference of the up and down quarks.

The simplest observable to measure the phase of the s wave multipole amplitude occurs for photoproduction (with unpolarized photons) from targets polarized normal to the reaction plane [16]. The polarized target asymmetry, $A_T(\theta^*) = p_T \sigma_T(\theta^*)/\sigma_0(\theta^*)$, where p_T is the target polarization, θ^* is the pion CM emission angle, $\sigma_0(\theta^*)$ is the unpolarized cross section, and $\sigma_T(\theta^*)$, the polarized target cross section, is:

$$\begin{aligned} \sigma_T(\theta) &= 3q \sin \theta^* [T_0 + T_1 \cos \theta^*]/k \\ T_0 &= |E_{0+}| |M_{1+} - E_{1+}| \sin(\chi - \chi_p) \end{aligned} \quad (4)$$

where $q(k)$ are the pion (photon) CM momenta, M_{1+} and E_{1+} are p wave multipoles [15] and in the limit that the p wave phases χ_p are small $T_1 \cong 0$. Estimates using the p wave effective range parameters [5] show that we can neglect the contributions of the p wave phases. After a precise experiment is performed small corrections for these terms can be made; their presence will show up in the T_1 term in Eq. 4. To measure the phase the unpolarized cross

section as well as an experiment with polarized photons must be performed to obtain the magnitudes of the multipoles.

To estimate the magnitude of the polarized target asymmetry one needs the magnitudes of the s and p wave multipoles. For the $\gamma p \rightarrow p\pi^0$ reaction an (unpublished) empirical fit to the most accurate threshold data [17] has been used. For the $\gamma p \rightarrow n\pi^+$ multipoles theoretical calculations [18] have been used. The magnitudes of the estimated polarized target asymmetries A_T are shown in Fig. 2. For the $\pi^0 p$ channel A_T is small for energies below the $\pi^+ n$ reaction threshold. For higher energies A_T rises rapidly with the phase χ due to the two step $\gamma p \rightarrow n\pi^+ \rightarrow p\pi^0$ charge exchange reaction. For the $n\pi^+$ channel the magnitude of A_T is $\sim 1\%$ not too far from threshold.

State of the art experiments which measure the target asymmetry A_T are feasible. One needs to use a tagged photon beam with energy resolution of < 1 MeV. Tagged intensities of $\sim 10^7$ photons/sec/MeV can be achieved for a limited range of photon energies, e.g. ~ 20 MeV [19] along with frozen spin targets [20] of 5 cm length ($L \sim 2 \cdot 10^{30} \text{ cm}^{-2} \text{ sec}^{-1}$). With a large array π^0 detector with good energy resolution [21] one can separate the π^0 decay γ rays from the hydrogen and heavier elements in the target with a total π^0 detection efficiency in excess of 10%. In 100 hours of data collection one can obtain a statistical error $\delta A_T \sim 0.5\%$. It is important that the systematic error should not be significantly larger. This is sufficient to measure the phase in the $p\pi^0$ channel above the $n\pi^+$ threshold where it is dominated by the two step $\gamma p \rightarrow n\pi^+ \rightarrow p\pi^0$ charge exchange reaction. As can be seen from Fig. 2 this is a small error for energies a few MeV above the $n\pi^+$ threshold. To measure the $p\pi^0$ phase below the $n\pi^+$ threshold a significant improvement in the accuracy will be required. This will have to be obtained primarily by an increase in the overall efficiency and in the intensity of the photon flux; an intense laser backscattering facility with this capability has been proposed recently [22].

For the $\gamma p \rightarrow n\pi^+$ reaction one can detect the neutrons which, in the region just above threshold, are emitted in a narrow cone. Since the cross sections are much larger in the charged pion channels one obtains a statistical error $\delta A_T \sim 0.1\%$ in 100 hours of data

collection. As can be seen from Fig. 2 for photon energies ~ 160 MeV this would be a relative error of $\sim 10\%$.

Measurements of the s wave scattering lengths $a(n\pi^+ \rightarrow p\pi^0)$, $a(p\pi^0)$ and $a(n\pi^+)$ can be utilized to check isospin conservation by comparison to data obtained with pion beams in different charge states, e.g., $a(p\pi^-)$ [7]. Finally we note from Eq. 1 that a measurement of $a(p\pi^0)$ is closely related to the πN sigma term [3,8]. It is still necessary to extrapolate to the Cheng-Dashen point [3,8] but some of the experimental problems associated with extrapolating from higher energies are eliminated. However the question of isospin symmetry violations in the πN sigma term [4,9] must still be taken into account.

In conclusion we have proposed a new technique [23] to measure low energy πN interactions based on the phase measurement of the near threshold amplitudes in photo (electro) pion production. The method proposed here can be used to test the predictions of chiral dynamics for the s wave πN scattering lengths, and the πN sigma term, and to test isospin symmetry which has been predicted to be broken by the difference of the up and down quark masses [4,9]. These experiments are feasible using existing state of the art technology.

Acknowledgements

It is a pleasure to acknowledge the contribution of F. E. Low in the derivation of the extended Fermi-Watson theorem and S. Weinberg for discussions of isospin violation in the πN system. This work benefited from helpful discussions with many colleagues including T. W. Donnelly, T. S. H. Lee, E. J. Moniz, U. Meißner, B. Norum and T. P. Welch. This work was supported in part by the Department of Energy.

REFERENCES

- [1] S. Weinberg, *Phys. Rev. Lett.* **17**, 168 (1966).
- [2] *Current Algebras and Applications to Particle Physics*, S. L. Adler and R. F. Dashen, Benjamin, N.Y. (1968).
- [3] *Dynamics of the Standard Model*, J. F. Donoghue, E. Golowich, and B. R. Holstein, Cambridge University Press (1992).
- [4] S. Weinberg, *Transactions of the New York Academy of Sciences, Series II* **38** (I.I.Rabi Festschrift), 185 (1977).
- [5] G. Höhler, *Pion Nucleon Scattering*, Landolt- Bornstein Vol 9, Springer Verlag(1983).
- [6] *Proceedings of the IV International Symposium on Pion-Nucleon Physics and the Structure of the Nucleon*, Bad Honef, Germany, Sept. 1991: π N Newsletter #5, March 1992, and #6, April 1992, R. E. Cutkowsky, G. Hohler, W. Kluge, and B. M. K. Nefkens, editors.
- [7] W. Beer *et. al.* *Phys. Lett.* **B261**, 16 (1991).
- [8] J. Gasser, H. Leutwyler, and M. E. Sanio, *Phys. Lett.* **B253**, 252 (1991).
- [9] J. Gasser and H. Leutwyler, *Phys. Rep.* **87**, 77 (1982).
- [10] V. Bernard, N. Kaiser, and U. Meißner, Bern University preprint, *Phys. Lett.* **B309**, 421 (1993), and *Nucl. Phys.* **B383**, 442 (1992).
- [11] E. Fermi, *Suppl. Nuovo Cimento*, **2**, 17 (1955), K. M. Watson, *Phys. Rev.* **95**, 228 (1954).
The Fermi Watson theorem has been previously used to simplify the analyses of photo pion reactions.
- [12] Obtained in collaboration with F. E. Low.
- [13] The notation for the multipoles is E(M) signifies and electric (magnetic) multipole, the

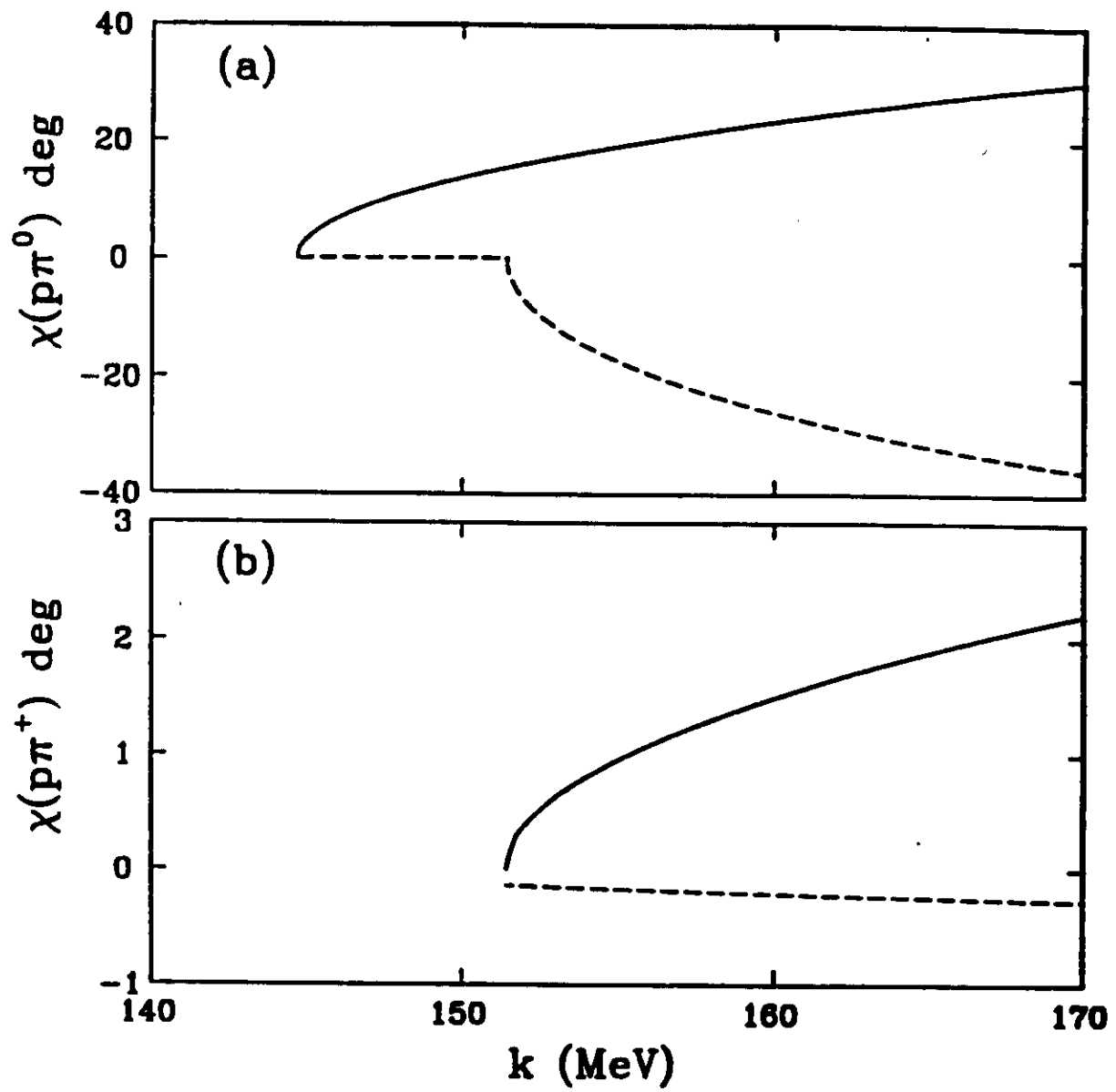
integer represents the angular momentum ℓ of the emitted pion, and the +/- refer to the total angular momentum $j = \ell \pm 1/2$. The s wave multipole is E_{0+} and the three p wave multipoles are M_{1+} , M_{1-} , and E_{1+} .

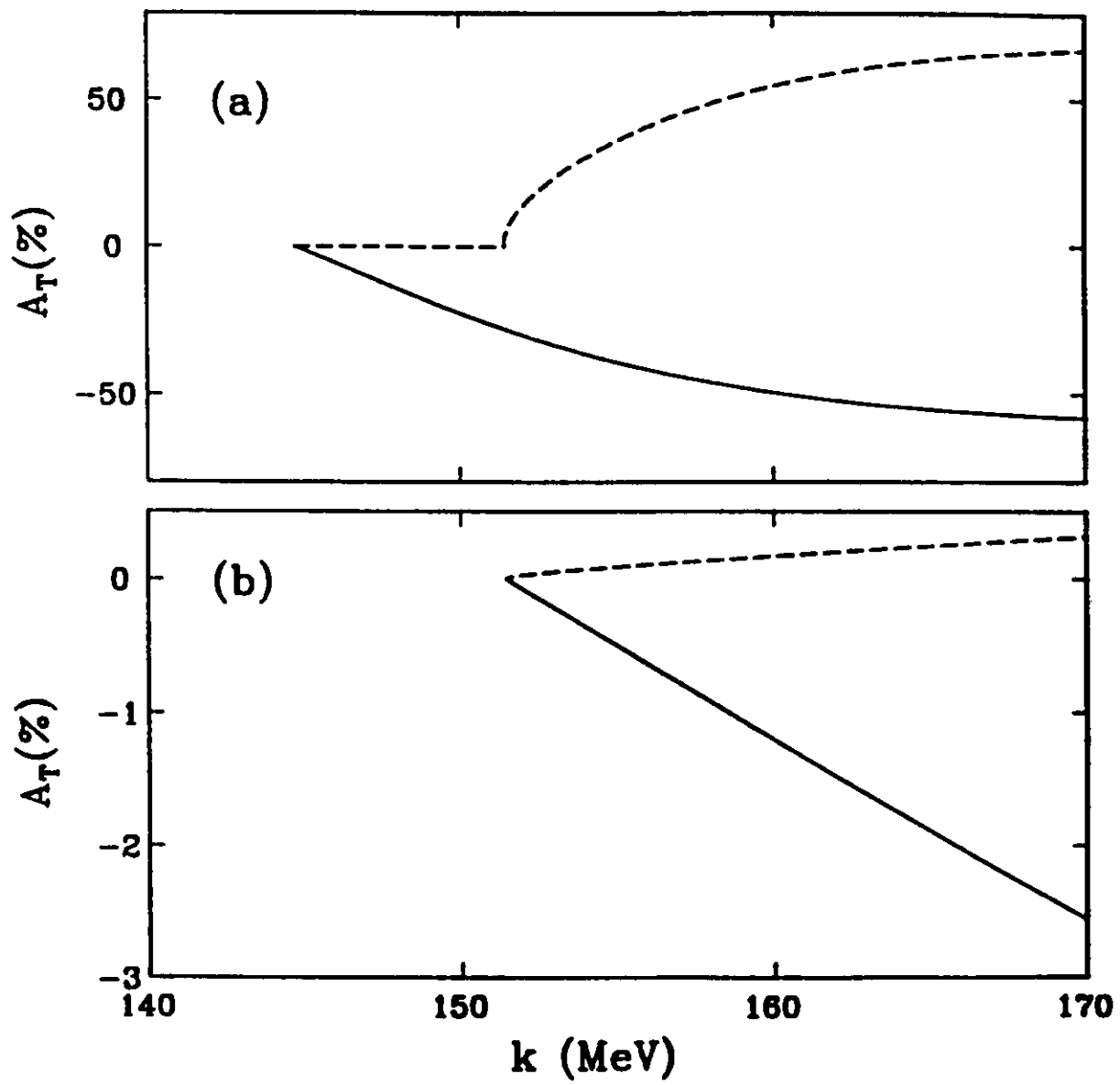
- [14] J. C. Bergstrom and E. L. Hallin, Phys. Rev. **C48**, 1508 (1993).
- [15] M. Benmerrouche and N. C. Mukhopadhyah, Phys. Rev. **D46**, 101 (1992).
- [16] A. S. Raskin and T. W. Donnelly, Annals of Phys. **191**, 78 (1989). D. Dreschel and L. Tiator, J. Phys. **G18**, 449 (1992).
- [17] R. Beck *et. al.* Phys. Rev. Lett. **65**, 1841 (1986).
- [18] S. Nozawa, T. S. H. Lee, and B. Blankleider, Phys. Rev. **C41**, 213 (1990).
- [19] J. D. Kellie *et. al.*, Nucl. Instr. and Methods, **A241**, 153 (1985).
- [20] H. Dutz *et. al.*, High Energy Spin Physics, Proceedings of the 9th International Symposium held at Bonn, FRG, September 1990. W. Meyer, E. Steffens, W. Lhiel, Editors, Springer-Verlag.
- [21] R. Novotny, IEEE Transactions on Nuclear Science, **38**, 379 (1991). D. Pocanic *et. al* PSI Proposal (1992).
- [22] B. Norum and T. P. Welch, An Intense Polarized Photon Source at CEBAF Hall B, Letter of Intent to CEBAF, April 1993.
- [23] During the course of this research S. Weinberg pointed out to me that the same principal was previously suggested to him by J. D. Bjorken in a private conversation [4].

FIGURES

FIG. 1. Phase angle $\chi(N\pi)$ estimates for the electric dipole amplitude E_{0+} versus photon energy for: (a) the $\gamma p \rightarrow \pi^0 p$ reaction and (b) the $\gamma p \rightarrow \pi^+ n$ reaction. In (a) the solid curve represents the phase shift, multiplied by 100, due to elastic $\pi^0 p$ scattering using $a(\pi^0 p) = .01/m_\pi$ (the smallest estimated value). The dashed curve is for the two step charge exchange $\gamma p \rightarrow \pi^+ n \rightarrow \pi^0 p$ process. In (b) the solid curve is for elastic $\pi^+ n$ scattering while the dashed curve is for the two step charge exchange process $\gamma p \rightarrow \pi^0 p \rightarrow \pi^+ n$. The effects of the $\gamma p \rightarrow \pi^0 p$ and $\gamma p \rightarrow \pi^+ n$ thresholds of 144.7 and 151.5 MeV can be seen in the curves.

FIG. 2. Estimated polarized target asymmetries, A_T (in %), versus photon energy for: (a) the $\gamma p \rightarrow \pi^0 p$ reaction for θ^* , the CM pion angle, of 30 degrees; and (b) the $\gamma p \rightarrow \pi^+ n$ reaction for $\theta^* = 90$ degrees. In (a) the solid curve, which is multiplied by 100, is due to elastic $\pi^0 p$ scattering only, calculated using $a(\pi^0 p) = .01/m_\pi$. The dashed curve includes the effects of the dominant two step charge exchange $\gamma p \rightarrow \pi^+ n \rightarrow \pi^0 p$ reaction. In (b) the solid curve represents the contribution due to elastic $\pi^+ n$ scattering. The dashed curve represents the contribution of the two step charge exchange contribution.





B Experimental Observables

In this appendix we present the observables in terms of the multipoles for the threshold $N(\gamma, \pi)$ reaction with linearly polarized photons and polarized targets[24], and indicate how they will be obtained from the data. The definitions presented in Sec. 2 will not be repeated here.

With the convenient choice for the polarization axis, target polarization transverses to the beam and transverse polarization of the beam at 45° relative to the target polarization we measure the observables σ , Σ , T and H in one experiment[43]

$$\sigma(\theta, \phi) = \sigma_0(\theta)(1 + \Pi_\gamma \Sigma(\theta) \sin 2\phi + P_T T(\theta) \cos \phi + P_T \Pi_\gamma H(\theta) \sin \phi)$$

The pion angle ϕ is defined by the direction of the target polarization (90°) and the beam polarization (45°).

Differential Cross Section:

$$\begin{aligned} \sigma_0(\theta) = \frac{p_\pi^*}{k_\gamma^*} \sigma'_0(\theta) &= \frac{p_\pi^*}{k_\gamma^*} (|E_{0+}|^2 + \frac{1}{2}|2M_{1+} + M_{1-}|^2 + \frac{1}{2}|3E_{1+} - M_{1+} + M_{1-}|^2 \\ &\quad + 2 \cos \theta \Re\{E_{0+}^*(3E_{1+} + M_{1+} - M_{1-})\} \\ &\quad + \cos^2 \theta \{|3E_{1+} + M_{1+} - M_{1-}|^2 \\ &\quad - \frac{1}{2}|2M_{1+} + M_{1-}|^2 - \frac{1}{2}|3E_{1+} - M_{1+} + M_{1-}|^2\}) \end{aligned}$$

Polarized Beam Asymmetry:

$$\Sigma(\theta) \cdot \sigma'_0(\theta) = \frac{3}{2} \sin^2 \theta \Re\{-3|E_{1+}|^2 + |M_{1+}|^2 - 2M_{1-}^*(E_{1+} - M_{1+}) + 2E_{1+}^* M_{1+}\}$$

Polarized Target Asymmetry:

$$\begin{aligned} T(\theta) \cdot \sigma'_0(\theta) &= 3 \sin \theta \Im\{E_{0+}^*(E_{1+} - M_{1+}) - \cos \theta (M_{1-}^*(E_{1+} - M_{1+}) - 4M_{1+}^* E_{1+})\} \\ &\approx 3 \sin \theta \Im\{E_{0+}^*(E_{1+} - M_{1+})\} \end{aligned}$$

Beam Target Double Polarization Asymmetry:

$$\begin{aligned} H(\theta) \cdot \sigma'_0(\theta) &= -\sin \theta \Im\{(E_{0+}^* - 3 \cos \theta M_{1-}^*)(3E_{1+} + 2M_{1-} + M_{1+})\} \\ &\approx -\sin \theta \Im\{E_{0+}^*(3E_{1+} + 2M_{1-} + M_{1+})\} \end{aligned}$$

From the ϕ_π^* distribution of the cross section obtained from a fit to the data one can disentangle the terms which go as $\sin(\phi)$, $\cos(\phi)$ and $\sin(2\phi)$. This will not only enable us to take data much faster but also to substantially reduce the systematic error.

The approximations made above neglect the phase of the p wave multipoles. This is an excellent approximation in this energy region due to the small πN shifts (see eg., ref. [29])

With other choices for the target polarization axis it is possible to measure the observables G and P, and with circularly polarized photons E and F. Only 6 of those 8 observables are linearly independent.

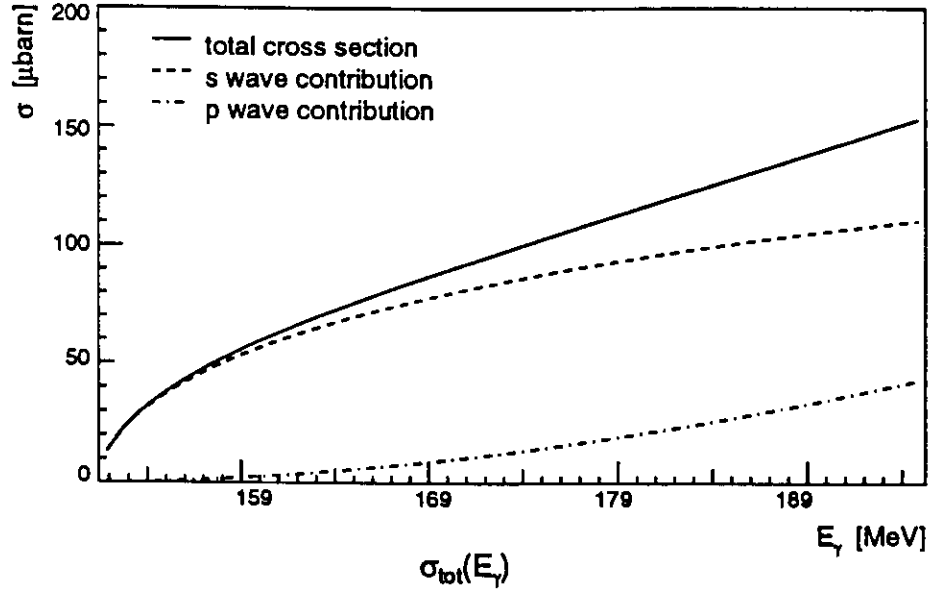


Figure 14: Contributions of the s and p wave multipoles to the total cross section.

C Future Measurements of the $p(\gamma, n)\pi^+$ Reaction

In order to complement the measurements of the $p(\vec{\gamma}, \pi^0)p$ reaction proposed here we will in the near future want to measure the reaction $\vec{\gamma}p \rightarrow \pi^+n$ at threshold using transversely polarized photons. To determine the amplitude of the multipoles at threshold we need to cover the energy range close enough to threshold to determine the E_{0+} contribution and high enough to separate the p-wave multipoles, which are expected to rise linearly with $p^* = k_\gamma^* p_\pi^*/m_\pi^2$. Calculations with the model of [25] show (see figs. 14 and 15) that it is sufficient to measure the differential cross section in the range of $10 \text{ MeV}/c < p_\pi^* < 100 \text{ MeV}/c$. Very close to threshold we expect

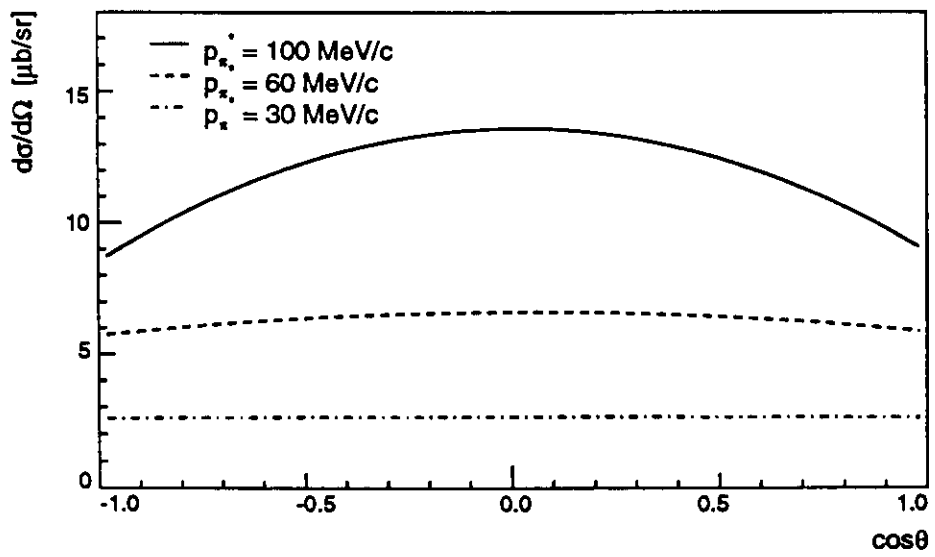


Figure 15: Angular Distribution.

only s-wave contributions, so we only have to measure the total cross section there.

Here we discuss the required detector resolutions, the estimates of count rates and the statistical uncertainties in the extracted multipoles and the magnitudes of the systematic uncertainties. It will be shown that due to the large cross section and the high quality of the CEBAF beam in addition to the coverage of the whole kinematical region by the detector the statistical uncertainties will be small compared to the systematic uncertainties. Accurate calibration of the neutron detection efficiency will reduce the most important source of systematic errors.

C.1 Kinematics and Detector Resolution

Near threshold the recoiling neutron is emitted within a narrow cone in the direction of the photon beam. Fig. 16 shows the kinematical situation. We have to cover a angular range of up to 35° to cover the desired energy range. For the forward and backward CM direction of the pion the uncertainty in the determination of the the pion CM angle θ_π^* is mainly caused by the position resolution of the neutron detector. In this region the momentum resolution is only used to separate the two different branches. At higher laboratory angles the θ_π^* resolution is determined by the momentum resolution.

To estimate the total resolution we reconstruct the CM angle as the weighted average of the two possible reconstructions:

$$\theta_\pi^* = \frac{\theta_1^*(p_n)}{(\Delta\theta_1^*(p_n))^2} + \frac{\theta_2^*(\theta_n)}{(\Delta\theta_2^*(\theta_n))^2}$$

where θ_1^* is the pion CM angle reconstructed with the neutron laboratory momentum p_n and θ_2^* is the pion CM angle reconstructed with the neutron laboratory angle θ_n .

Fig. 17 shows the resulting uncertainty calculated with gaussian error propagation and the assumed resolutions of

$$\frac{\Delta p}{p} = 10\%$$

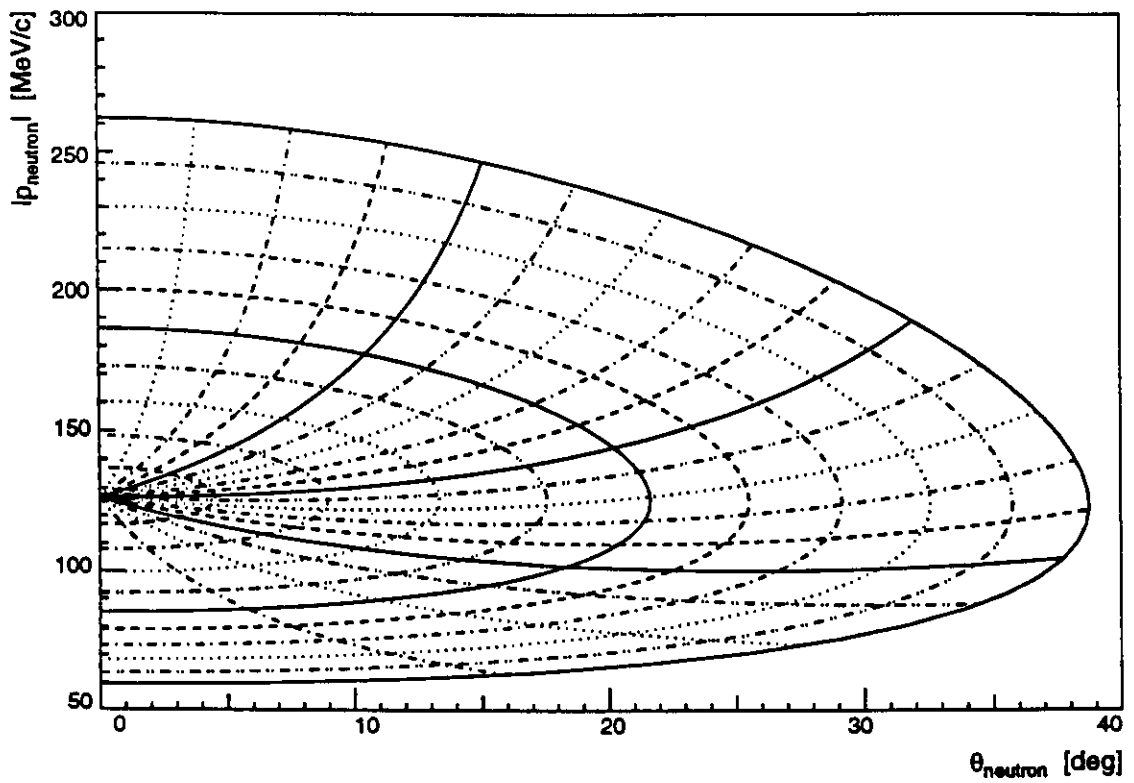


Figure 16: Kinematical region of the neutron momentum and neutron angle in the laboratory frame. The curves of constant CM momentum are drawn in steps of $10 \text{ MeV}/c$ from threshold up to $100 \text{ MeV}/c$ and the curves of constant CM angle are drawn in steps of 10° .

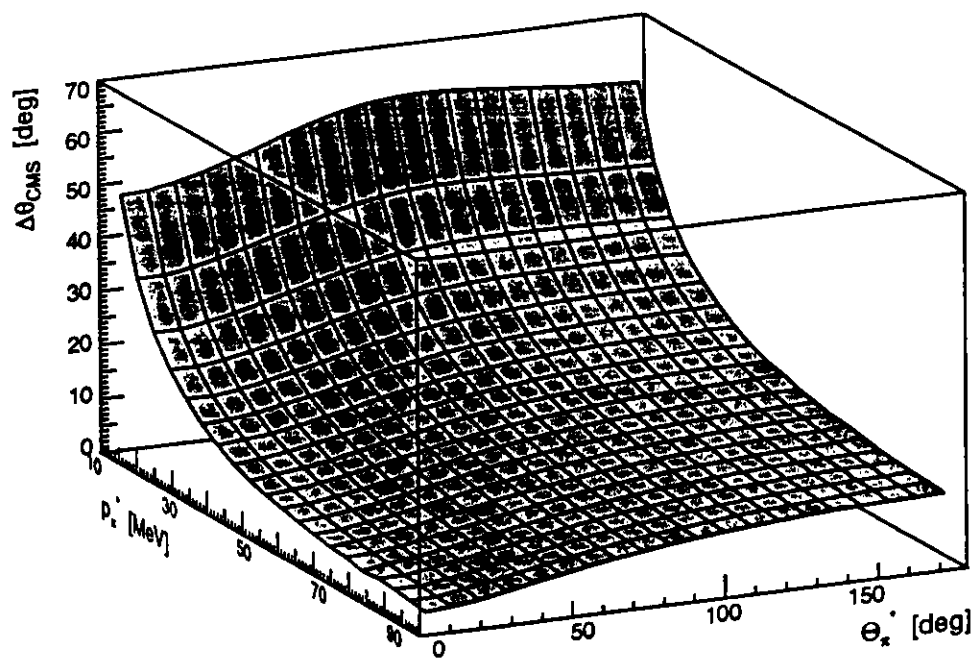


Figure 17: Error of the reconstructed CM angle θ_x^* .

$$\Delta\theta_n^{LAB} = 5^\circ$$

This angular resolution of better than 10° for $p_\pi^* > 30\text{MeV}/c$ is sufficient to measure the expected smooth angular distribution of

$$\frac{d\sigma(\theta, \phi)}{d\Omega} = (A + B \cdot \cos\theta + C \cdot \cos^2\theta) \cdot (1 + \Sigma(\theta) \cdot \cos 2\phi)$$

C.2 Neutron Detector

We propose to detect the neutrons with a scintillation detector which have the advantages of easy handling, fast timing, and homogeneous efficiency. To achieve an efficiency of $\approx 20\%$ we need a thickness of the scintillation material of 20cm . To cover the angular range of 35° we want to use an area of $70\text{cm} \times 70\text{cm}$ at a distance of 50cm from the target. A hole will be left in the middle of the detector to allow the $\vec{\gamma}$ beam to pass undetected. A thin veto scintillator will separate charged particles from neutrons.

To determine the interaction point of the neutron in the scintillator we will divide the scintillator into four slices each 5cm thick. The resulting uncertainty in the measurement of the flight length of $\pm 2.5\text{cm}$ is a large contribution to the uncertainty in the time of flight measurement. With a total flight length of $l = 50\text{cm}$ this contribution is

$$\frac{\Delta l}{l} = \frac{2.5\text{cm}}{50\text{cm}} = 5\%$$

As shown in fig. 16 the maximum momentum of the neutrons is $260\text{MeV}/c$. This correspond to an minimum time of flight of

$$t_{min} = \frac{l}{\beta \cdot c} = \frac{50\text{cm}}{26.7\% \cdot c} = 6.3\text{ns}$$

with an assumed time resolution of $\delta t = 400\text{psec}$ the resulting time of flight resolution is between 6.3% at $260\text{MeV}/c$ and 1.5% at $60\text{MeV}/c$. We expect

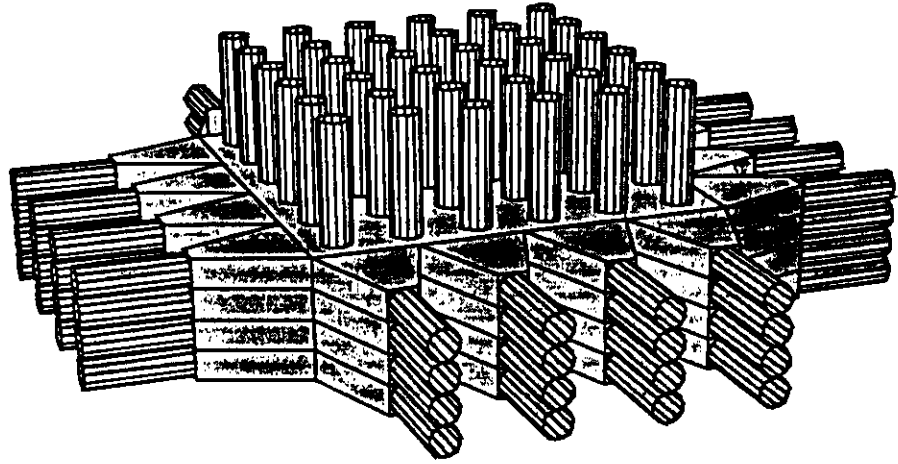


Figure 18: Preliminary design of the neutron detector. The detector consists of 4 homogeneous slices of scintillators in the dimensions $5\text{cm} \times 70\text{cm} \times 70\text{cm}$.

to achieve an overall momentum resolution of better than 10% over the whole momentum range, and of $\approx 6\%$ at $p_n = 130\text{MeV}/c$, where the reconstruction uncertainty is mainly determined by the momentum resolution.

With two-side readout of scintillators a position resolution of better than 4cm is possible. This corresponds to an angular resolution of better than 5° .

Fig. 18 shows the preliminary design of the neutron detector. In addition to the four-side readout of the scintillators we want to improve the time and position resolution by readout with a matrix of photomultipliers on the back. The photomultipliers of the matrix are mounted with an air gap between

multiplier and scintillation material so only direct light with an angle less than the angle of total reflection ($\alpha_{tot} = 39^\circ$ for NE110) hits the multipliers.

The use of direct light improves the time resolution. From the distribution of the detected light an additional improvement in the position resolution can be achieved. A similar detector design for the detection of protons has already been used[44]. Resolutions of $\sigma_x = 3-5mm$ and $\sigma_t = 150-250ps$ could be reached. Of course, these numbers cannot be reached for the detection of neutrons, but we expect an improvement in resolution in comparison with the usual design. Even without improvement of the resolution, this design has the advantage that the light of every neutron is seen by at least 6 photomultipliers. Accordingly, the calibration of the neutron efficiency is much less dependent of the discriminator thresholds of single photomultipliers.

C.3 Calibration of the Neutron Detection Efficiency

We want to calibrate the neutron efficiency by an independent simultaneous measurement. The $\bar{\gamma}$ beam quality allows us to use a thin target with $5mm$ radius, so a large fraction of the π^+ 's can leave the target. The pions will be detected by two pion counters, each consisting of a small plastic scintillator ($0.5cm \times 17cm \times 20cm$) to separate pions and protons by measurement of dE/dx and an BaF scintillator ($10cm \times 17cm \times 20cm$) (fig. 19). In the BaF scintillator the pions are stopped and are identified by their weak decay. The plastic scintillator readout is on the four sides, the BaF readout is a matrix of 3×3 photomultipliers on the back. With the pion momentum and energy measurement we can reconstruct the direction and energy of the neutron and calibrate the efficiency of the neutron counter.

C.4 Count rate estimates

For monte carlo simulations we used the values for the multipoles of [25]. The theoretical predictions and analyses are not widely spread so the cross sections used should be accurate enough for these estimates.

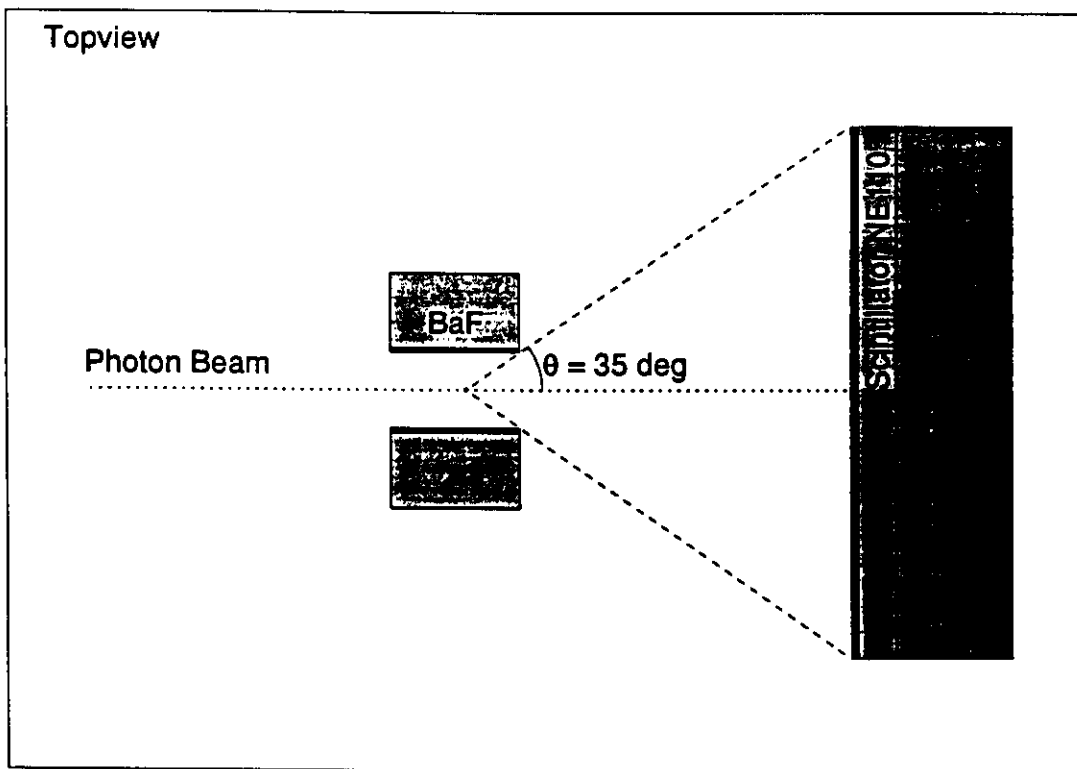


Figure 19: Position of the Scintillators for the Experiment

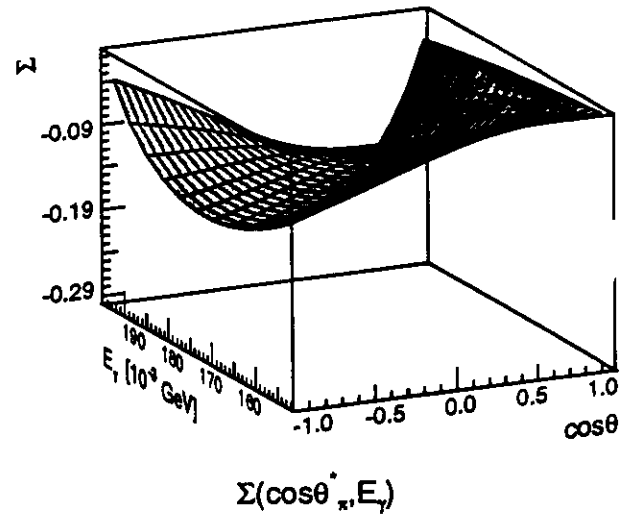
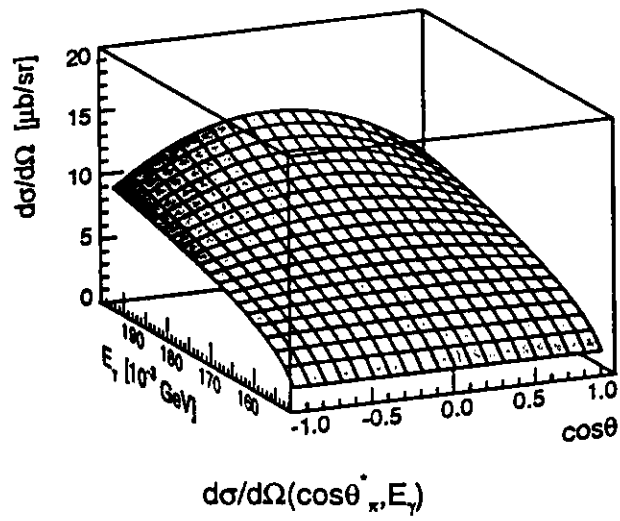


Figure 20: Cross section and polarized beam asymmetry.

Fig. 20 shows the calculated cross section. In the cross section we see the flat angular distribution by the s-wave at threshold and the emerging p-wave dominance at higher energies. We expect a polarized beam asymmetry of the order of up to 20%.

For the count rate estimation we used the following numbers for the tagged photon intensity, beam polarization and available beam time:

$$\begin{aligned} N_{tag} &= 10^5 \frac{Hz}{MeV} \\ \vec{P}_\gamma &= 90 \% \\ l_{target} &= 0.5 \text{ cm} \\ t &= 100 \text{ h} \end{aligned}$$

resulting in a tagged photon luminosity of $\mathcal{L} = 2 \cdot 10^{27} Hz/cm^2/MeV$. Fig. 21 shows the total number of counts we expect in 100h of beam time with a neutron efficiency of 20%.

We simulated the angular distribution and extracted the multipoles by fitting to the simulated data. Fig. 22 shows the result of the fit. It is clearly shown that the statistical uncertainty will be small in comparison to the systematic uncertainty introduced by the calibration of the detector. However, the ratios between the multipoles can be determined with very high precision and constitute an accurate test of the theoretical predictions.

C.5 Conclusion

We plan to measure the reaction $\gamma p \rightarrow \pi^+ n$ using the Compton $\vec{\gamma}$ source and a scintillator detector. We plan to detect both the produced pion and the recoiling neutron so we can calibrate the apparatus by two independent measurements of the cross section.

The detection of the neutron enables us to cover 4π of the CM solid angle in the region from threshold up to a momentum of 100MeV/c above threshold so the statistical uncertainty will be small. The moderate required tagging rate

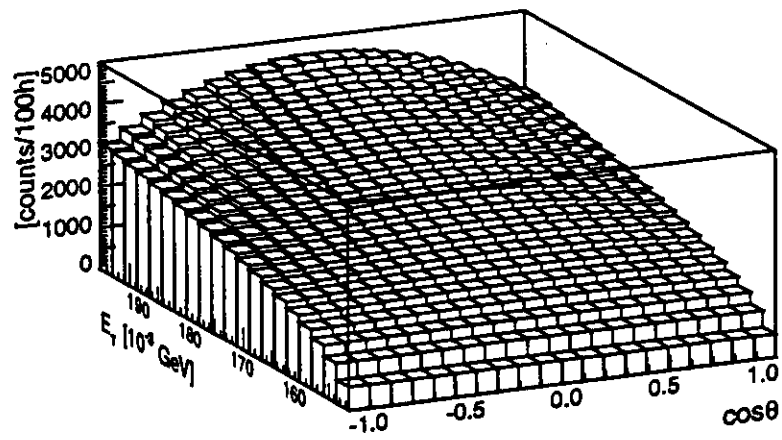


Figure 21: Count rate estimate.

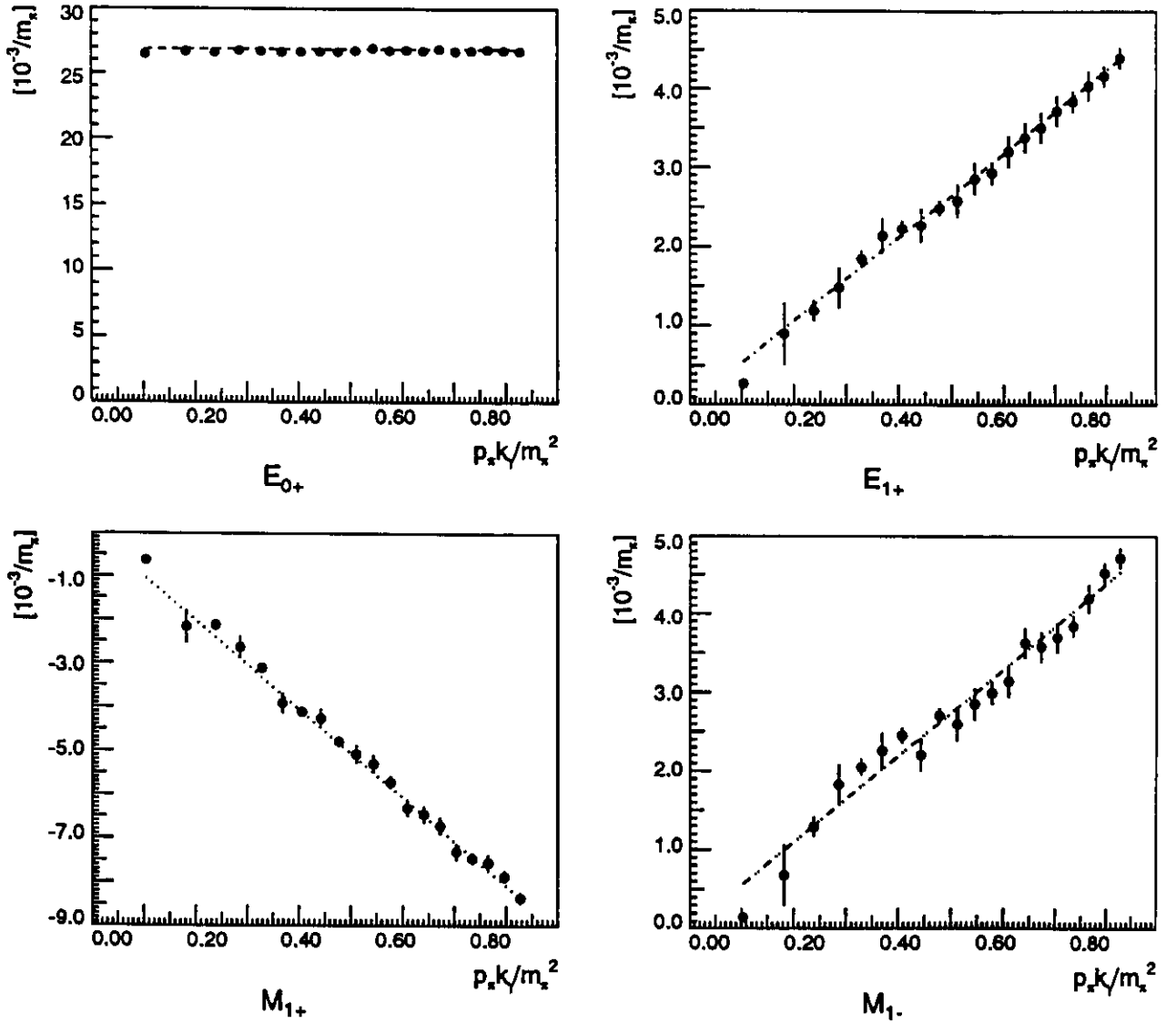


Figure 22: Simulation: reconstructed Multipoles with statistical error bars

of 10^5 Hz/MeV reduces the problem of multiplicity in the tagging hodoscope so a clear kinematical identification is possible.

HAZARD IDENTIFICATION CHECKLIST

CEBAF Experiment: _____ Date: April 13, 1994

Check all items for which there is an anticipated need—do not check items that are part of the CEBAF standard experiment (HRSE, HRSH, CLAS, HMS, SOS in standard configurations).

Cryogenics <input type="checkbox"/> beamline magnets <input type="checkbox"/> analysis magnets <input checked="" type="checkbox"/> target <input type="checkbox"/> drift chambers <input type="checkbox"/> other	Electrical Equipment <input checked="" type="checkbox"/> cryo/electrical devices <input type="checkbox"/> capacitor banks <input type="checkbox"/> high voltage <input type="checkbox"/> exposed equipment	Radioactive/Hazardous Materials List any radioactive or hazardous/toxic materials planned for use: _____ _____
Detector Windows <input type="checkbox"/> inside diameter <input type="checkbox"/> operating pressure <input type="checkbox"/> window material <input type="checkbox"/> window thickness	Memorable Gas or Liquids (incl. target) type: <u>Hydrogen</u> flow rate: _____ capacity: _____	Other Target Materials <input type="checkbox"/> Beryllium (Be) <input type="checkbox"/> Lithium (Li) <input type="checkbox"/> Mercury (Hg) <input type="checkbox"/> Lead (Pb) <input type="checkbox"/> Tungsten (W) <input type="checkbox"/> Uranium (U) <input type="checkbox"/> Other (list below) _____ _____
Vacuum Vessels <input type="checkbox"/> inside diameter <input type="checkbox"/> operating pressure <input type="checkbox"/> window material <input type="checkbox"/> window thickness	Radioactive Sources <input type="checkbox"/> permanent installation <input type="checkbox"/> temporary use type: _____ strength: _____	Large Mech. Structure/System <input type="checkbox"/> lifting devices <input type="checkbox"/> motion controllers <input type="checkbox"/> scaffolding or elevated platforms <input type="checkbox"/> other
Lasers type: <u>Ar-ion</u> wattage: <u>25</u> class: <u>1V</u> Installation <input checked="" type="checkbox"/> permanent <input type="checkbox"/> temporary Use <input type="checkbox"/> calibration <input type="checkbox"/> alignment <input checked="" type="checkbox"/> photon source	Hazardous Materials <input type="checkbox"/> cyanide plating materials <input type="checkbox"/> scintillation oil (from) <input type="checkbox"/> PCBs <input type="checkbox"/> methane <input type="checkbox"/> TMAE <input type="checkbox"/> TEA <input type="checkbox"/> photographic developers <input type="checkbox"/> other (list below) _____ _____ _____	Notes: Requires installation of detector in front of CLAS. _____ _____ _____ _____